



Seismic risk assessment of a large metropolitan area by means of simulated earthquakes

Eliana Fischer¹ · Giovanni Barreca² · Annalisa Greco³ · Francesco Martinico⁴ · Alessandro Pluchino^{1,5} · Andrea Rapisarda^{1,5,6}

Received: 28 April 2022 / Accepted: 26 April 2023 / Published online: 11 May 2023
© The Author(s) 2023

Abstract

The determination of seismic risk in urban settlements has received increasing attention in the scientific community during the last decades since it allows to identify the most vulnerable portions of urban areas and therefore to plan appropriate strategies for seismic risk reduction. In order to accurately evaluate the seismic risk of urban settlements it should be necessary to estimate in detail the seismic vulnerability of all the existing buildings in the considered area. This task could be very cumbersome due to both the great number of information needed to accurately characterize each building and the huge related computational effort. Several simplified methods for the assessment of the seismic vulnerability of existing buildings have been therefore presented in the literature. In order to estimate the occurrence of damage in buildings due to possible seismic phenomena, the published studies usually refer to response spectra evaluated according to seismic events expected in the territory with assumed probabilities. In the present paper seismic events are instead simulated using a modified Olami–Feder–Christensen (OFC) model, within the framework of self-organized criticality. The proposed methodology takes into account some geological parameters in the evaluation of the seismic intensities perceived by each single building, extending the approach presented in a previous study of some of the authors. Here, a large territory in the Sicilian oriental coast, the metropolitan area of Catania, which includes several urbanized zones with different features, has been considered as a new case study. Applications of the procedure are presented first with reference to seismic sequences of variable intensity, whose occurrence is rather frequent in seismic territories, showing that the damage can be progressively accumulated in the buildings and may lead to their collapse even when the intensities of each single event are moderate. Moreover, statistically significant simulations of single major seismic events, equivalent to a given sequence in terms of produced damages on buildings, are also performed. The latter match well with a novel a-priori risk index, introduced with the aim of characterizing the seismic risk of each single municipality in the considered metropolitan area. The proposed procedure can be applied to any large urbanized territory and, allowing to identify the most vulnerable areas, can represent a useful tool to prioritize the allocation of funds. This could be a novelty for risk policies in many countries in which public subsidies are currently assigned on a case-by-case basis, taking into account only hazard and vulnerability. The use of an a-priori

risk index in the allocation process will allow to take into due account the relevant role of exposure.

Keywords Seismic vulnerability · Urban areas · Gis · Numerical simulations · Self-organized criticality

1 Introduction

Investigating on the seismic response of buildings at metropolitan scale allows to identify the most vulnerable portions of urban areas and therefore to plan opportune strategies for seismic risk reduction.

In order to evaluate the seismic risk of urban settlements it should be necessary, in principle, to estimate the seismic vulnerability of all the buildings in the considered area. This estimate needs in-depth knowledge of the geometric and mechanical characteristics of the load-bearing structures of each building and requires the calculation of appropriate safety coefficients with respect to possible seismic events (Ramos and Lourenço 2004; Greco et al. 2018, 2020a, b; Senaldi et al. 2010; Maio et al. 2015; Polese et al. 2013). Taking into account a great number of buildings this task would require a large amount of data and a huge computational effort. This is not always easy to achieve especially in countries where awareness of the importance of seismic risk mitigation is still weak. It is therefore fundamental that decision-makers have available simplified planning tools which provide reliable results even if they are based on reduced information about the buildings present in the area under examination.

Due to the great interest in simplified vulnerability assessment several scientific studies have been published in the last decades (Gaudio et al. 2015; Zuccaro and Cacace 2015; Riedel et al. 2015; Maio et al. 2016; Matassoni et al. 2017; Lu et al. 2014; Silva and Horspool 2019; Hancilar et al. 2010). In particular Lagomarsino and Giovinazzi proposed two models: a macroseismic and a mechanical one, to be used, respectively, with macroseismic intensity hazard maps and when the hazard is provided in terms of peak ground accelerations and spectral values (Lagomarsino and Giovinazzi 2006). The two methods, denoted by LM1 (macroseismic) and LM2 (mechanical), have been included in the Risk-UE project and taken into account by many countries in the preparation of opportune sheets which assess the seismic vulnerability of existing buildings at different detail level.

Among recent studies available in the literature, Boukri proposed simplified methodological and operational approaches to assess urban seismic vulnerability and socio-economic losses at urban scale in Algeria (Boukri et al. 2018). Vicente estimated the physical damage scenarios, economical and human losses related to the vulnerability assessment of the old city center of Faro, in Portugal (Vicente et al. 2014). Del Gaudio (Gaudio et al. 2020) analyzed the data concerning the damage observed in about 25,000 residential reinforced concrete buildings inspected in the aftermath of the most devastating earthquakes occurred in Italy between 1976 and 2012 and determined different classes of buildings and the relevant vulnerability and fragility curves. Ferreira et al. (1996) presented a simplified methodology to evaluate the seismic vulnerability of 91 reinforced concrete buildings affected by recent earthquakes with different macroseismic intensities. Zhai et al. (2019) proposed a GIS-based seismic hazard prediction system for urban earthquake disaster prevention planning. Vargas Alzate et al. (2020) developed a method for the seismic risk assessment under assigned earthquake records which considers the nonlinear dynamic

response of the structures and takes into account some uncertainties related to the loads, the geometry of the buildings and the mechanical properties of the materials. The role of biases, discrepancies and uncertainties in the hazard and vulnerability components of three cities in Columbia has been investigated in Hoyos and Hernandez (2022). The seismic hazard has been recently evaluated for Puerto Vallarta metropolitan area (Jaimes et al. 2022), Plovdiv (Stefanov et al. 2023), Mexico City (Gómez-Bernal et al. 2023) also taking into account social vulnerability and economic losses. The difference between the objective seismic risk of buildings in an urban area and the one perceived from their inhabitants has been analyzed with the aim of understanding the critical elements that prevent the adoption of relevant seismic risk mitigation measures (Fischer et al. 2022). All these works are based on capacity spectra and refer to expected seismic events probabilities in the territory in question. However, there are computational models that, interfaced with territorial maps in the GIS environment, allow simulating the effects of seismic excitations in the various sites of interest with a good approximation. Among others, Zhao et al. (2007) obtained simulated waveforms using an impulse point source in a 3D velocity structure to synthesize seismograms of ground motion as Green's function for any prescribed rupture scenario and source functions. Jin and Smerzini (2022) recently proposed a 3D physics-based numerical approach to generate ground shaking scenarios for strong earthquakes in the Thessaloniki area.

Some of the authors of this paper have recently published a study (Greco et al. 2019) in which the seismic events were simulated using a modified version of the Olami–Feder–Christensen (OFC) model (Olami et al. 1992), recognized in the scientific literature as suitable for reproducing seismic stress in a given territory within the context of Self-Organized Criticality (Jensen 1998). In the cited study, the OFC model has been conveniently combined with urban and geological datasets and applied to the estimation of the seismic vulnerability of a small urban center on the south-eastern coast of Sicily. Furthermore, instead of taking into account only single earthquake of a certain intensity, the typical approach used in urban vulnerability studies, sequences of seismic events are accounted for. This aims at modeling realistic seismic activities in which large seismic events are often preceded and followed (foreshock and aftershock) by an intense seismic activity of variable intensity and duration (Omori Law) (Omori 1894; Utsu et al. 1995; Baiesi and Paczuski 2004; Kossobokov and Nekrasova 2017). For example, the main shock of magnitude M 5.9 (Richter Scale) occurred in L'Aquila (Italy) on April 6, 2009, was the largest event of an intense activity spanning from December 2008 to the end of 2012.

In the present paper, the methodology proposed in Greco et al. (2019) has been extended assuming a more detailed correlation between geological characteristics of the soil and the seismic intensity perceived from the buildings in the selected area and performing numerical simulations for both the case of single or repetitive seismic events. Moreover, a larger territory which includes urbanized zones with different features has been chosen as case study: the metropolitan area of Catania, which includes 25 municipalities of different size with more than two hundred thousand buildings in total. A local a-priori seismic risk index for each municipality, based on “Crichton's Risk Triangle” (Crichton 1999), has also been proposed. The risk has been evaluated considering the Hazard associated to the geological features, the Exposure proportional to the number of buildings in each municipality and the Vulnerability related to the characteristics of the buildings.

The analysis of the effects of seismic excitations has been carried out by associating to the intensity of the earthquake at each site a prediction of the damage on the various buildings located in the territory under consideration. In defining the intensity perceived by the single building, characteristic parameters of the soil, such as the acceleration referred to the

rigid ground and the slope of the ground, have been taken into account. These parameters can in fact significantly affect the intensity of the seismic shock at the base of the buildings.

In the applicative section, the results of many simulations for both the case of single or repetitive seismic events of variable intensity are shown. With reference to sequences of seismic events it will be shown that the damage can be progressively accumulated in the buildings and may lead to their collapse even if the intensities of each single event are moderate. Furthermore, the effects, in terms of damage on buildings, of major single earthquakes of selected magnitude are evaluated. In order to provide statistically significant results 100 earthquake simulations for each of the considered magnitudes have been performed and an average damage for each municipality has been evaluated.

The proposed seismic simulations allow classifying the municipalities in terms of average damage level and the obtained results are in good agreement with the introduced risk index. In this way, the proposed seismic simulation allows a risk-based approach, depending on simulated and reliable scenarios, different from the hazard map, which has been adopted so far in the policies for risk reduction management (Saunders and Kivilgton 2016).

The performed simulations also allow to identify, within each municipality, in which areas the buildings are mostly damaged by possible seismic events. This result, eventually matched with information regarding road infrastructures, could be extremely useful in planning appropriate measures for risk management. In particular, the obtained results could be useful in defining planning actions aimed at reducing seismic risk, such as prioritization of funds, individuation of key renewal areas, inclusion in the urban planning documents of the results of vulnerability and seismic risk assessment studies, urban transformation and development provisions in relation to risk maps. This could be done at municipal level with direct effects on land use plans.

It is also worth noting that the proposed approach could be applied to different urbanized territories with variable geological and structural features and can be enriched with further details regarding both the characteristics of the soil and of the buildings.

2 The simulated seismic events

In this paper, the seismic activity dynamics has been simulated by means of a modified version of the well-known Olami–Feder–Christensen (OFC) model (Caruso et al. 2007). By means of the adoption of this model, it is possible to reproduce the statistical characteristics of several earthquakes (Omori 1894) as briefly summarized hereafter. The area under investigation can be modeled as a two-dimensional rectangular lattice of sides L and H with N nodes and K links (see Fig. 1), where the introduction of a few numbers of long-range connections makes it equivalent to a small-world graph (Watts and Strogatz 1998). A seismogenic force F_i (seismic stress) is applied on each node and all the forces on the nodes are uniformly increased until one of them reaches a critical value and becomes “active.” At this stage, the loading is no longer increased and an earthquake begins: A fraction α of the force of the active nodes is transferred to the neighbors, which can consequently become active and transfer forces to other neighbors until the dynamics stops, producing an earthquake of size S . The latter is defined through the number of nodes activated during the dynamics, colored in red in Fig. 1, and represents the energy released by the seismic event. After a certain transient, these rules (under an opportune calibration of the control parameters, see Caruso et al. 2007) drive the system into a critical state, where large seismic

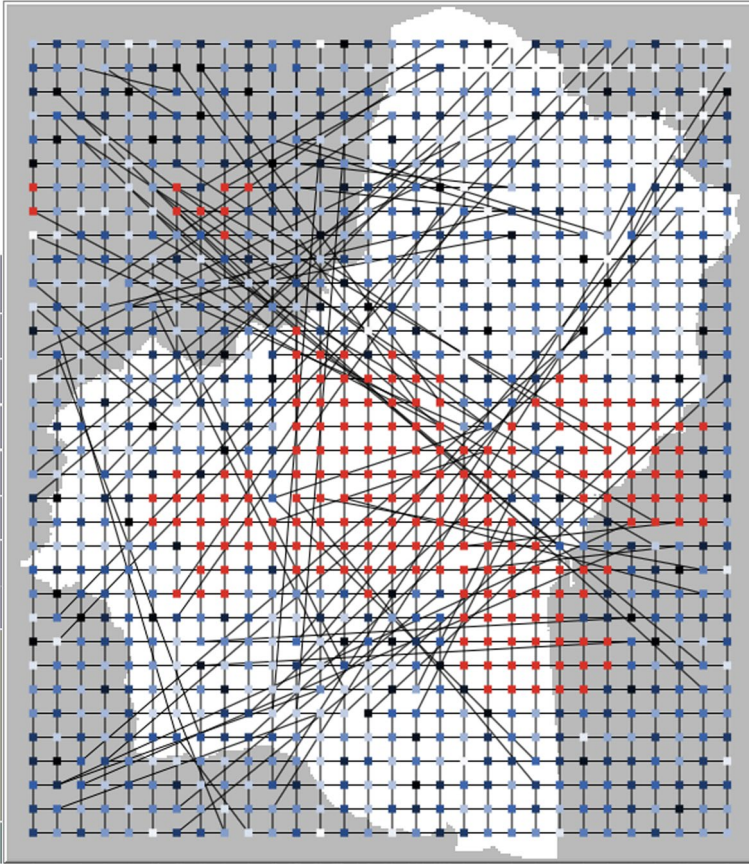


Fig. 1 Small world $L \times H$ regular lattice of the OFC model with $N=1020$ nodes and $K=1976$ links, with some long-range connections. The color of nodes in gray-scale are proportional to their seismic stress. Nodes in red represent the S sites activated by an earthquake of size S . The profile of the metropolitan area of Catania, chosen as case study, is distinguishable in the background. See text for further details

events can occur with a certain probability. The presence of seismogenic faults present in the considered territory can be modeled through nodes (called “fault nodes”) which can be activated with a greater probability.

Typically, the OFC model is considered for reproducing sequences of earthquakes distributed over time, but our modified model is able to simulate also the impact of single events of a particular chosen intensity. In the present study, the intensity of the seismic input is considered as a continuous parameter in the range 1–12 according to the European Macroseismic Scale (EMS-98) (EMS 1998). It is important to point out that due to the sub-surface geological setting, amplifications of the seismic input with respect to rigid soil conditions can occur and therefore the same intensity can be differently perceived by the buildings present in the considered territory. The size S of an earthquake in the OFC model can be related to the corresponding intensity I in the EMS-98 by means of the magnitude $M = \ln S$ as described in Greco et al. (2019). In particular in the following, reference will be made to the empirical relation $I(M) = 1.71M - 1.02$ which takes into account the comparison between the magnitude scale and the EMS-98 one (Musson et al. 2010).

In the present study, the peak ground acceleration a_g at rigid soil (PGA, see Sect. 4.2) and a slope parameter a_s will be considered as geological and topographic parameters, so that the perceived seismic intensity in a given area will be defined as:

$$I(M, a_g, a_s) = (1.7M - 1.02)(1 + a_g)a_s \quad (1)$$

where $a_g \in [0, 1]$ and, according to the Italian technical code, $a_s = \begin{cases} 1.0 & \text{for } 0^\circ \leq s \leq 15^\circ \\ 1.2 & \text{for } 15^\circ < s \leq 30^\circ \\ 1.4 & \text{for } s > 30^\circ \end{cases}$

and s is the local slope of the ground with respect to the horizontal layout. Equation (1) clearly shows that both the rigid ground acceleration and the slope can sensibly amplify the intensity of the seismic event.

3 Damage on buildings produced by seismic events

The seismic vulnerability assessment of a single building require the knowledge of its structural, geometrical and mechanical characteristics together with information on the geological characteristics of the site. These parameters are not often readily available, in particular when the analyses have to be performed at urban scale. However, also in absence of detailed data, an approximated vulnerability index can be still estimated. For example, according to the macroseismic model presented in Lagomarsino and Giovinazzi (2006), suitable ranges $[V_{\min}, V_{\max}]$ for the vulnerability index can be assumed, as reported in Table 1, for masonry and reinforced concrete buildings. As it can be observed the vulnerability index varies from a minimum value $V_{\min} = -0.02$ for structures with high earthquake resistant design (E.R.D) to a maximum value $V_{\max} = 1.02$ in total absence of E.R.D. In the present study, an initial vulnerability V_0 of each type of building is assigned at the beginning of the simulation by matching the information contained in a given urban GIS data set and randomly choosing the value in the related interval of vulnerability presented in Table 1. This initial vulnerability will be successively updated considering the damage progressively accumulated in the building. The damage μ_D in a building of vulnerability index

Table 1 Reference vulnerability of buildings

Typologies	Building type	Vmin	Vmax
Masonry	Rubble stone and earth bricks	0.62	1.02
	Simple stone	0.46	1.02
	Massive stone	0.3	0.86
	Masonry with old bricks	0.46	1.02
	Masonry with r.c. floors	0.3	0.86
	Reinforced /confined masonry	0.14	0.7
Reinforced concrete	Frame in r.c. (without E.R.D)	0.3	1.02
	Frame in r.c. (moderate E.R.D.)	0.14	0.86
	Frame in r.c. (high E.R.D.)	-0.02	0.7
	Shear walls (without E.R.D)	0.3	0.86
	Shear walls (moderate E.R.D.)	0.14	0.7
	Shear walls (high E.R.D.)	-0.02	0.54

V caused by a certain seismic intensity $I(M, a_g, a_s)$ is evaluated by means of the analytical function provided in Lagomarsino and Giovinazzi (2006) as follows:

$$\mu_D[I(M, a_g, a_s)] = 2.5 \left[1 + \tanh\left(\frac{I(M, a_g, a_s) + 6.25V - 13.1}{Q}\right) \right] \tag{2}$$

According to what suggested in Greco et al. (2019), the ductility index Q for masonry buildings has been assumed equal to 2.3, judged to be representative for buildings not specifically designed to have ductile behavior. For reinforced concrete buildings the value $Q=2.6$ has been assumed since, although these are more ductile than masonry buildings, most of them have been designed without taking into account the earthquake loadings. Damage in buildings may be caused either by a strong seismic event or during repetitive sequences of earthquakes of moderate intensity. The damage $\mu_D \in [0, 5]$ produced by a single seismic event is directly computed by means of Eq. (2) while in the case of repetitive events it is assumed that, for each building, the damage progressively cumulates according to the relation $\mu_D^{TOT} = \sum \mu_D$. At the same time, the updated vulnerability V_{new} is here defined as:

$$V_{new} = V_0 \left(1 + \frac{\mu_D^{TOT}}{5} \right) \tag{3}$$

This means that ensuing earthquakes can progressively cause damage on buildings, increasing the parameter μ_D^{TOT} (which starts from 0 at $t=0$). The value of μ_D^{TOT} classifies the status of each building: In particular, it is considered “slightly (or moderately) damaged” when $0.5 \leq \mu_D^{TOT} < 2$, “heavily (or very heavily) damaged” when $2 \leq \mu_D^{TOT} < 4$ and “destroyed when $4 \leq \mu_D^{TOT} \leq 5$ [30].

The knowledge of the total damage for each building after each seismic input allows to globally visualize the areas in the considered territory having the same level of damage and may therefore be very significant in an urban management.

4 The case study of Catania metropolitan area (CMA)

In this section, we present Catania Metropolitan Area (CMA) located along the east coast of Sicily (Italy) which will be considered in the rest of this paper as a case study. The area has size 893 sqkm and contains a set of twenty-five municipalities, including the main city of Catania (Fig. 2). It considers the current extension of the conurbation that has developed, in the last 40 years, by a progressive northbound radial expansion of the built up area toward the slopes of Mount Etna and along the coast.

The nature of the present built up heritage of CMA is the result of this growth process that has progressively included the smaller existing agro-towns and the nearby countryside forming an uninterrupted urban settlement (Greca et al. 2011; Rosa and Privitera 2013). This explains the considerable heterogeneous age of the buildings in the examined area.

4.1 Description of the urban GIS dataset

Starting from the 50s and early 60s, the city of Catania was characterized by a considerable demographic growth. Consequently, the city had a period of great urban expansion

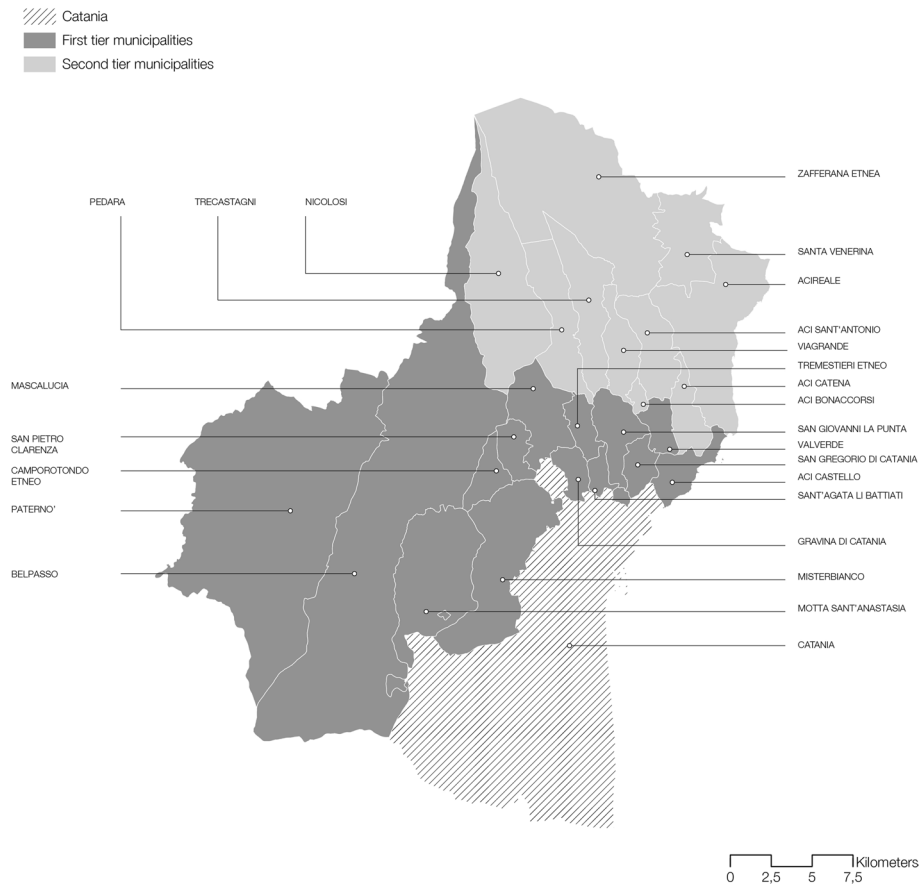


Fig. 2 Municipality of Catania is shown together with the first tier and the second tier municipalities

amplified by a strong attitude toward property speculation by medium and small entrepreneurs in the building sector. From the early 1970s, there was a gradual spillover of the development toward the municipalities located north of the city border, along the volcano slopes and the coastline (Dibben 2008).

This diffusion of residential buildings outside the municipal limits of the main city was due to several factors. These include: The refusal of the low quality residential model that was prevailing in the decaying historic center and in the new districts built in 1960–70; the increased availability of private cars and the connected upsurge in vehicular mobility; better environmental and scenic conditions of the surroundings areas of the main city.

The twenty-five municipalities of the metropolitan area of Catania, which represent the core of the urban agglomeration around the eponymous municipality, feature a population of 786,234 inhabitants (January 2020) and a total number of 206,916 buildings. About 60% of the CMA population lives in the municipalities closer to the main city that can be considered as its residential districts (Greca and Martinico 2017). These municipalities can be classified in two groups: A “first tier,” around the administrative borders of the main city, and a “second tier”, which includes the outer municipalities and extends along the south-eastern side of Mt Etna (Fig. 2). The municipalities of

the “first tier” are: Motta Sant’Anastasia, Misterbianco, Paternò, Belpasso, Camporotondo, San Pietro Clarenza, Sant’Agata Li Battiati, Mascacchia, Tremestieri, San Giovanni La Punta, San Gregorio, Valverde, Aci Castello. The “second tier” includes: Nicolosi, Pedara, Trecastagni, Zafferana Santa Venerina, Viagrande, Aci Bonaccorsi, Aci Sant’Antonio, Aci Catena, Acireale, Gravina di Catania.

In Table 2, data relating to urbanized areas for each municipality are reported. In detail the overall area is indicated for each municipality; the built-up area represents the surface covered exclusively by the buildings and it covers the 5.68% of the whole CMA. The urbanized area covers 21,000 ha, 42% of the entire CMA territory. Approximately 45.5% of the building stock was built before 1964, while between 1964 and 1985, the process of urban expansion showed an increase in the built-up areas of 36%, largely without any protection measures against seismic risk (Table 3). Only since 1981, according to the Italian National Law no.741/1981, the Regions were obliged to issue «rules for the adaptation of general and detailed urban planning tools in force, as well as the criteria for the formation of urban planning tools for preventing seismic risk». This means that only about 16% of buildings are built with characteristics of resistance to seismic stress and that a considerable number of buildings was built without a formal authorization, a practice which has been quite common in Southern Europe and in Italy (Allen et al. 2004; Chiodelli et al. 2020).

The study, based on the available historical cartographies, has produced a comprehensive GIS map of the growth of urban settlements in study area, starting from the early 1900s up to 2016.

The cartography, issued by the Regional Territorial Department, retrieved from the GIS Sicilian Regional Website (SITR) have been superimposed on historical maps of the urban fabric. Urban growth had been mapped by using available cartographies corresponding to five main dates (1928, 1964, 1985, 1999 and 2016). In the resulting GIS map each existing building features the date in which it is present in the corresponding map. This allows a rough estimate of the construction period of each building.

The available Numerical Technical Map contains also the volumetric information relating to the mapped buildings, together with the height and surface data.

The information obtained through the support of the GIS tool allowed the identification of the initial vulnerability level according to the geometric characteristics of the single building, height and width, and construction date; the slope with respect to the ground and the peak acceleration are the geological characteristics that will amplify the seismic effects on the building in case of occurrence of an earthquake (see Sect. 4.2). Due to the asymmetric frequency distribution of the initial vulnerability, instead of using the average it is more reasonable to characterize the municipalities with the most expressed value (mode) of the initial vulnerability of their buildings, as shown in Table 4.

Specifically, the municipalities of Gravina, Paternò, Nicolosi, Acireale and Trecastagni are found in the higher range of 0.76–0.68. Paternò has the largest percentage of buildings, 41%, built before 1928, 30% between 1965 and 1985, and the remaining 29% between 1985 and 1999. Acireale has the largest percentage of buildings, 41%, built before 1928; another 40% has been built between 1928 and 1985. Nicolosi has 90% of the buildings built before 1985 and the same percentage holds for Gravina di Catania while 61% of Trecastagni has been built before 1985. These values show a vulnerable built heritage, as the building characteristics do not meet the design criteria of the anti-seismic legislation. A very significant building stock, which as it can be observed in Table 3 is equal to 80%, was built without seismo-resistant criteria.

Table 2 Catania metropolitan area land cover: Total area per single town (GIS data-set); Total built-up area and percentage of built-up area of total surface per single town (GIS data-set); surface of urbanized census tracts per single town and percentage of total surface of urbanized census tract (Source: elaboration of the authors on data ISTAT, 2011 - Italian National Institute of Statistics, cartography and territory); percentage of urbanized census tract per single town (Source: elaboration of the authors on data ISTAT, 2011 - Italian National Institute of Statistics, cartography and territory)

Municipalities	Total area (ha)	Built-up area (ha)	Built-up area (%total surface)	Urbanized (ha)	Urbanized (%total surface)	Built-up area (%Urbanized)	
1	Aci Bonaccorsi	172	20.21	11.79	115.18	66.80	17.64
2	Aci Castello	871	65.35	7.51	374.85	43.06	17.43
3	Aci Catena	853	70.79	8.30	343.88	40.29	20.59
4	Aci Sant'Antonio	1433	72.79	5.08	569.74	39.75	12.78
5	Acireale	4043	235.01	5.81	1764.53	43.64	13.32
6	Belpasso	16,633	158.47	0.95	1551.93	9.33	10.21
7	Camporotondo E	655	15.89	2.43	103.74	15.83	15.33
8	Catania	18,290	1104.15	6.04	6295.37	34.42	17.54
9	Gravina di Catania	515	65.43	12.70	392.04	76.12	16.69
10	Mascalucia	1628	127.85	7.85	1452.13	89.20	8.80
11	Misterbianco	3768	202.05	5.36	930.56	24.70	21.71
12	Motta S. Anastasia	3571	52.70	1.48	283.29	7.93	18.60
13	Nicolosi	4265	49.78	1.17	434.14	10.18	11.47
14	Paternò	14,468	145.59	1.01	562.11	3.89	25.90
15	Pedara	1923	79.95	4.16	1036.22	53.87	7.72
16	S. Giovanni la Punta	1085	104.31	9.62	933.99	86.10	11.17
17	San Gregorio	565	57.11	10.11	300.50	53.19	19.01
18	San Pietro Clarenza	627	25.08	4.00	201.70	32.16	12.44
19	Santa Venerina	1903	34.67	1.82	506.69	26.63	6.84
20	S. Agata li Battiati	312	34.88	11.16	262.55	84.02	13.29
21	Trecastagni	1916	59.72	3.12	568.87	29.70	10.50
22	Tremestieri Etneo	652	66.384	10.19	520.04	79.80	12.77
23	Valverde	552	32.30	5.85	261.11	47.29	12.37

Table 2 (continued)

	Municipalities	Total area (ha)	Built-up area (ha)	Built-up area (%total surface)	Urbanized (ha)	Urbanized (%total surface)	Built-up area (%Urbanized)
24	Viagrande	1009	37.74	3.74	474.67	47.02	7.95
25	Zafferana Etnea	7687	52.221	0.68	776.54	10.10	6.72
	Total CMA	89,397	2971	5.68	21,016	42.20	14

Table 3 Numerical and percentage increase in the building stock by time interval

Period	Increase	Percentage (%)	Cumulative (%)
Before 1928	59,053	28.54	28.54
1928–1964	37,369	18.06	46.60
1964–1985	76,249	36.85	83.45
1985–1999	21,892	10.58	94.03
After 1999	12,353	5.97	100

The time span within which the city grew the most and without the adoption of seismic building regulations are highlighted in bold

Table 4 Mode (most expressed value) of the initial vulnerability (V_0) per municipality

Mode of initial vulnerability per municipality									
Aci Bonaccorsi	0.67	Belpasso	0.64	Misterbianco	0.66	San G. LPunta	0.52	Trecastagni	0.68
Aci Castello	0.62	Camporotondo	0.62	Motta SA	0.60	San Gregorio	0.19	Tremestieri	0.52
Aci Catena	0.62	Catania	0.64	Nicolosi	0.69	San Pietro C	0.51	Valverde	0.53
Acireale	0.68	Gravina	0.76	Paternò	0.70	Sant'Agata LB	0.54	Viagrande	0.66
AciSant'Antonio	0.62	Mascalucia	0.52	Pedara	0.52	Santa Venerina	0.57	Zafferana	0.60

4.2 Geological framework and seismotectonic

The city of Catania and its metropolitan area are located in a relatively complex geo-tectonic region of Eastern Sicily, which encompass part of the Mt. Etna volcano and of the Catania-Gela foredeep domain (Fig. 3a). Mt. Etna is a Quaternary polygenic volcano formed close to the suture zone between the Africa and Europe plates and its origin has been associated to the activity of a regional-scale tectonic boundary (Doglioni et al. 2001; Gvirtzman and Nur 1999), the Malta Escarpment. Accordingly, crustal faulting and associated fracturing favored magma to ascend through the lithosphere up to the Sicily's Ionian coast. In the last 500 kyr, volcanic products have accumulated over a Pleistocene clayey substratum to build a composite strato-volcano. Throughout the history of Mt. Etna, four volcanic phases have been recognized (see Branca et al. 2008 and Fig. 3b): Basal Toleiithic (500–330 kyr), Timpe (220–110 kyr), Valle del Bove (110–60 kyr), and Stratovolcano (60–15 kyr). In the southern sector of the Catania metropolitan area, Quaternary basin-fill sedimentary rocks consisting of fluvial to marine successions of clays, sands, and conglomerates widely outcrop (Fig. 3b). The foredeep system's inner portion is presently buried beneath the Mt. Etna volcano, and its top-surface has been reconstructed using bore-hole and geophysical data (Branca and Ferrara 2013).

The investigated area, which encompasses the administrative territories of 25 municipalities, can be divided into two domains based on the outcropping rocks; a northern domain, characterized by a rigid bedrock of volcanic units and a southern one, characterized by a soft bedrock of sedimentary origin. In this frame, the urbanized portion of the considered municipalities is primarily based on a rigid volcanic bedrock except for those located near the border between the northern (volcanic) and the southern (sedimentary) domains. Among these, parts of the urban areas of Belpasso, Motta S. Anastasia, Misterbianco, Aci Castello, and the southern portion of the Catania urban settlement, are based on a soft sedimentary bedrock. According to the reconstructed top-surface of the foredeep system beneath the Mt. Etna volcano (see Branca and Ferrara 2013), a system of paleo fluvial incisions, carved on the Pleistocene sediments, is buried under the southern side

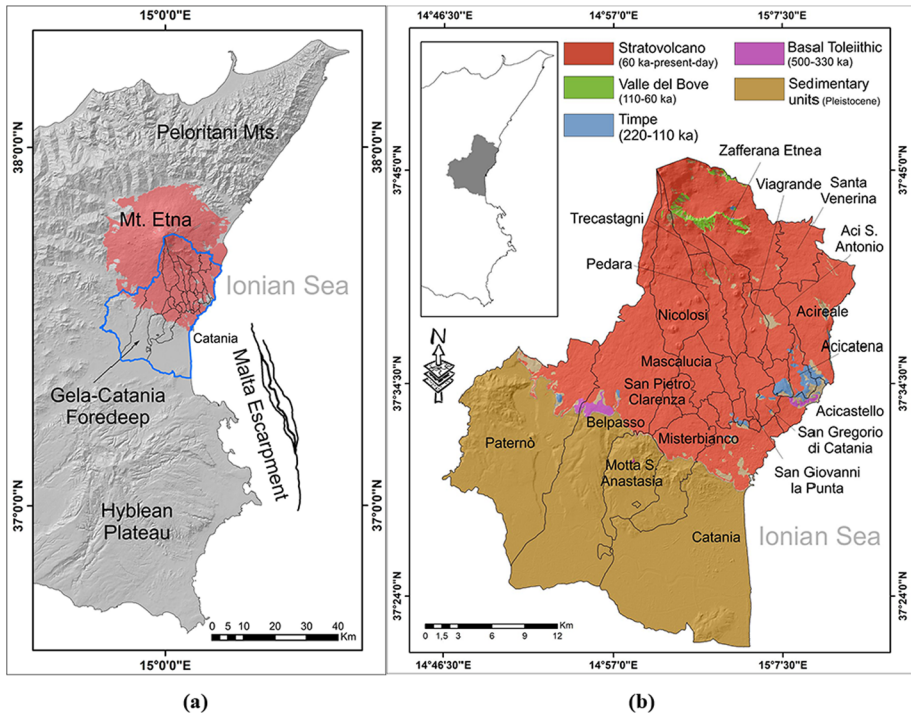


Fig. 3 **a** Investigated sector (blue polygon) framed in the tectonic context of Eastern Sicily. The studied region encompasses part of the Mt. Etna volcanic district (in the north) and of the Gela-Catania foredeep (in the south). Major regional-scale active faults are reported given their vicinity with the study area. **b** Geological map of the study area displaying the bedrock where the several analyzed urban areas are based. The Mt. Etna volcanic phases are from Branca et al. (2008)

of the volcano. The fluvial incisions were then progressively filled by the lava flow units erupted during the growth of the Mt. Etna volcano, resulting in a complicated subsurface stratigraphic setting. The thickness of the stiff volcanic units might vary greatly depending on their vicinity to the axis of the buried fluvial channels.

This aspect could have considerable implications on the behavior of the bedrock under dynamic conditions (i.e., during an earthquake) since site amplification of seismic waves is also a function of the subsurface rock layering and of the thickness of the rigid bedrock. These local geological effects, known as “site effects,” can amplify or de-amplify the seismic ground motion, producing differences in the shaking intensity (Bard and Bouchon 1985; Bard et al. 1988). The investigated sector lies in a rather tectonically unstable area where local and regional tectonics interact with each other at different rates. Local tectonics is largely concerned with the dynamic of the Mt. Etna volcano and particularly of its eastern flank, where volcano-tectonic and gravity-driven processes take place simultaneously (Azzaro et al. 2013). Gravity-related deformation gave rise to a large sliding area across whole eastern side of the volcano (Rasà et al. 1996; Rust and Neri 1996). As evidenced by geodetic data (Puglisi and Bonforte 2004; Bonforte and Puglisi 2006) and interferometric studies (Froger et al. 2001; Lundgren et al. 2004), the sliding area is characterized by a seaward motion of several blocks at a rate in the order of the cm/yr (Bonforte et al. 2011). The spreading toward the Ionian Sea is generally accommodated by (i) ground rupturing

along shallow discontinuities mainly developed at the northern and southern boundaries of the sliding block or (ii) by a reactivation of pre-existing tectonic structures (Azzaro et al. 2013).

The ensuing deformation field is therefore characterized by variously oriented fault systems (Fig. 4a), whose recent activity makes the eastern slope of the volcano the most tectonically active region of the volcanic edifice (Azzaro et al. 2011). A prominent set of active faults, locally known as the Timpe Fault System (TFS in Fig. 4a), occur at the north-eastern corner of the investigated area with an NNW-SSE direction. The system consists of at least 20 fault segments (Barreca et al. 2013), which were responsible in the last centuries for relatively shallow yet damaging earthquakes of low magnitude (Azzaro et al. 1989). The intense tectonic activity along the system is demonstrated by the occurrence of multiple shallow earthquakes (<5–6 km) of medium–low magnitude ($M < 4.5$) (Azzaro et al. 2011).

Most of the tectonic structures of the TFS have been then identified as active and capable faults by ISPRA (Istituto Superiore per la Protezione e la Ricerca Ambientale) and included in the ITHACA (ITaly HAZard from CAPable faults) dataset (<http://sgi2.isprambiente.it/ithacaweb/viewer>). The South Fault System (SFS in Fig. 4a, see Barreca et al. 2013), accommodates deformation along the southern border of the SE-ward sliding sector of Mt. Etna. The system is composed of four non-seismogenic fault branches (see Barreca et al. 2013 and Fig. 4a). Although local tectonics might contribute to the seismic hazard of the investigated region, a major seismotectonic role is attributed to the occurrence of regional-scale tectonic structures and particularly to the late Quaternary reactivation of the Malta Escarpment (Gambino et al. 2021). The Malta Escarpment (Fig. 3a), is a NNW-SSE trending tectonic lineament located in the near-offshore of eastern Sicily. Seismic exploration in the marine realm (Gambino et al. 2021; Gutscher et al. 2016), highlighted the recent

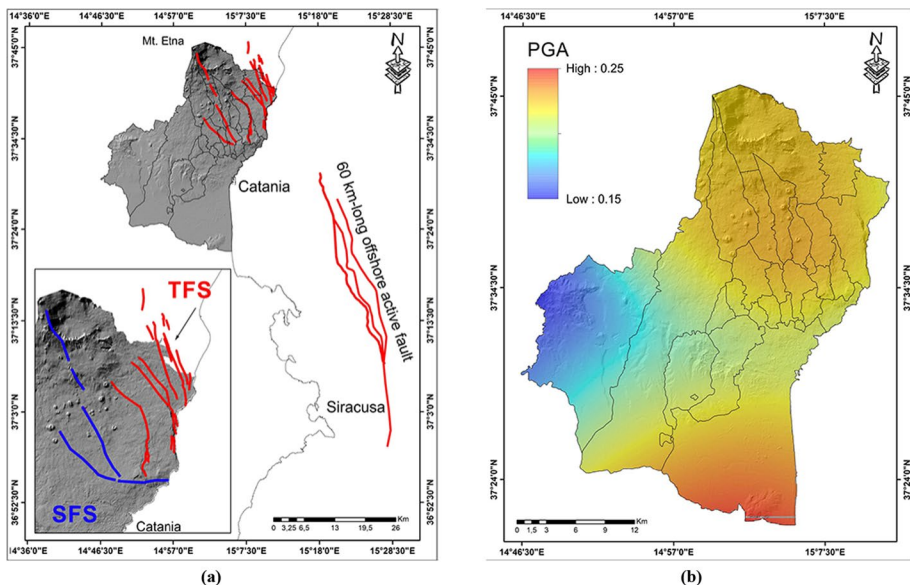


Fig. 4 **a** Major local and regional-scale active faults slicing across or nearby the investigated sector. The north-eastern sector is actively deformed by fault belts (in red) and **b** Map of PGA (Peak Ground Acceleration) for the investigated area

activity of the northern sector of the Malta Escarpment, which manifests mainly off Catania (in the north) and Siracusa (in the south) with seafloor displacement along three fault segments. Among these, the longest (~60 km-long) and most continuous fault segment might generate $M > 7$ earthquakes. According to historical catalogs (CPTI15, see Rovida et al. 2016), Eastern Sicily is one of the most seismically hazardous regions of Italy having experienced large earthquakes in the past centuries such as the February 4, 1169, and the January 11, 1693, events. The latter seismic event is commonly reported as the strongest earthquake of the Italian Peninsula ($I_0 = X/XI$ MCS and M_w 7.4).

According to the Seismic Hazard Map of Italy [MPS04, see Stucchi et al. 2004], the seismic hazard of a region is defined in terms of predicted PGA (Peak Ground Acceleration), the maximum horizontal acceleration expressed by a fraction of the gravity acceleration g (9.8 m/s^2). The expected PGA is computed through ground-motion predictive equations (GMPE), where magnitude (M), epicentral distance (R), soil conditions, and a specific spectral period (T) are considered. For the MPS04, three sets of GMPE (Sabetta and Pugliese 1996; Ambraseys et al. 1996; Malagnini et al. 2002, 2000) were adopted in a log-three approach to evaluate epistemic uncertainty.

The resultant seismic hazard map is expressed by the 10% probability of exceedance in 50 years of the calculated PGA, assuming a rigid soil with S-waves velocity in the 30 m-depth (V_{s30}) $> 800 \text{ m/s}$ (see point 3.2 of NTC/2008 NTC 2008) and a flat topographic surface (Meletti et al. 2006). In this frame, the Italian territory has been classified into four seismic zones according to the range of calculated PGA. Available database, containing the standard values of a_g and related uncertainties (<http://zonesismiche.mi.ingv.it/elaborazioni/download.php>) for the Sicilian territory, was exploited to derive the PGA distribution for the investigated sector. Georeferenced data points format (0.02° space-array), were then transformed in a continuous function (Grid) by using the Kriging interpolation method operated into the ARCGIS® platform. The resulting map (Fig. 4b), displays how the PGA values vary for the considered region ranging from 0.15 to 0.25 g (seismic zone 2). As previously stated in Sect. 2, the local values of PGA and ground slope with respect to the horizontal layout have been considered as input data to calculate the perceived seismic intensity I in Eq. (1).

5 Calibration of the model

A further calibration of the proposed model for earthquakes simulations is needed in order to allow a proper interaction between the OFC lattice and the buildings of the chosen dataset. This can be obtained by tuning the value of an appropriate control parameter f_B , representing the fraction of randomly chosen buildings around each node of the lattice, through a comparison of the damage produced by a simulated seismic scenario with real observed data. Since, according to the Italian seismic hazard map (<http://zonesismiche.mi.ingv.it>), the considered CMA has a seismic risk very similar to the territory of L'Aquila, the reference data are chosen as those related to the seismic sequences occurred at L'Aquila in April 2009.

A seismic scenario similar to the one occurred at L'Aquila in 2009 has been reproduced within our model and reported in Fig. 5. This seismic sequence exhibits 1000 seismic events in 10 days with three shocks of magnitude greater than M 5.

According with a procedure already tested in Greco et al. (2019), the comparison between the damage produced by the simulated seismic scenario and those really observed

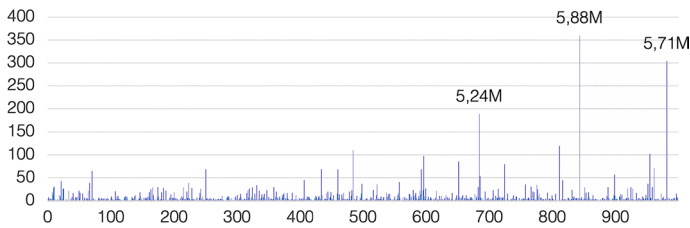


Fig. 5 Simulated seismic scenario similar to the one occurred in L'Aquila in 2009

in L'Aquila (Kawashima et al. 2010; Bosi et al. 2009; Carocci 2012; Decanini et al. 2009) allows to calibrate the value of the control parameter f_B . Table 5 reports the percentages of heavily damaged and destroyed buildings for the seismic scenario of L'Aquila compared with the same data obtained for the municipality of Catania, calculated performing different earthquake simulations in correspondence of increasing values of f_B (going from 0.35 to 0.44). As it can easily be noticed, damages increase with f_B and the most similar percentages for both the heavily damaged buildings (13.09%) and destroyed buildings (29.78%) is observed for the value $f_B = 0.37$. Therefore, this value will be chosen as the reference one. Notice that, once fixed f_B , all the parameters of the proposed model have been properly calibrated in order to find the optimal values allowing us to proceed with the simulation scenarios of the next section.

6 Simulation results

In this section, two different sets of simulations are presented: three scenarios with multiple earthquakes sequences of variable average intensity and three scenarios with single earthquakes of increasing intensity.

6.1 Multiple earthquakes scenarios

Let us start with three seismic sequences with earthquakes of different intensities, which allow investigating their effects in terms of accumulated damage on the buildings in the considered area.

In particular, the seismic sequences have duration 10 days inside the critical state and, after a transient of 600 events, exhibit 100 events per day. The “low intensity” seismic scenario has no events of magnitude greater than M 5; the “medium intensity” seismic scenario shows one event with magnitude greater than M 5; the “high intensity” seismic scenario includes two events of magnitude greater than M 5.

Figure 6 considers the low intensity seismic scenario. The plot in the top panel reports the increase in the total damage caused in the urban area by the chosen sequence of 1000 seismic events, whose sizes are shown in the bottom panel. The sequence is characterized by 25 earthquakes of magnitude between 3 and 4, 7 earthquakes of magnitude between 4 and 5, and no earthquake of magnitude greater than 5.

The total number of events (EV) cumulated up to days 1, 4, 7 and 10 are displayed in Table 6 for three different intervals of magnitude. In the same table, the corresponding percentages of slightly damaged (SDB), highly damaged (HDB) and destroyed (DB) buildings

Table 5 Comparison of the damage effects of the real seismic scenario of L'Aquila (2009) and a simulated scenario restricted only to the municipality of Catania (to make more reliable the comparison), for increasing values of the control parameter f_B

L'Aquila 2009	Heavily damaged buildings (%)	Destroyed buildings (%)	Heavily damaged + destroyed buildings (%)
Real data	17.40	24.30	41.70
Catania municipality (simulation)	Heavily damaged buildings (%)	Destroyed buildings (%)	Heavily damaged + destroyed buildings (%)
$f_B=0.35$	13.45	34.63	48.08
$f_B=0.36$	13.93	36.03	49.96
$f_B=0.37$	13.09	29.78	42.87
$f_B=0.38$	13.53	38.19	51.72
$f_B=0.39$	13.11	39.22	52.33
$f_B=0.40$	13.64	39.07	52.71
$f_B=0.41$	13.43	39.86	53.29
$f_B=0.42$	15.73	58.70	74.73
$f_B=0.43$	15.71	60.12	75.83
$f_B=0.44$	15.89	61.56	77.45

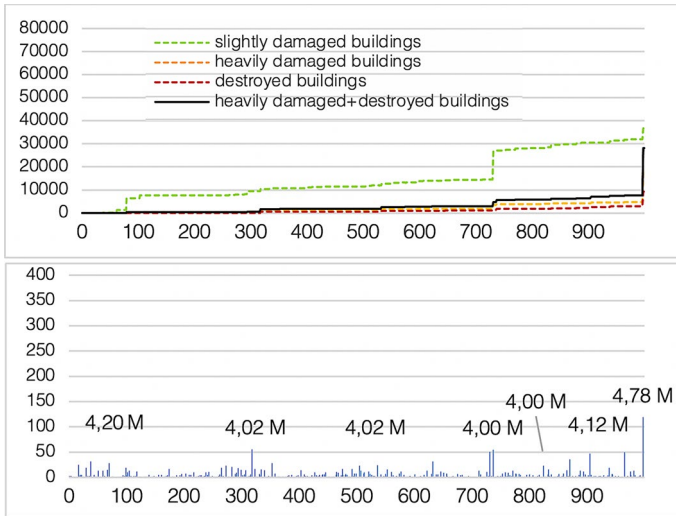


Fig. 6 Low intensity seismic scenario: The number of damaged and destroyed buildings are reported, in the top panel, as function of 1000 seismic events, whose sequence is shown in the bottom panel

Table 6 Low intensity seismic scenario: number of seismic events of different magnitude and percentages of slightly damaged (SDB), highly damaged (HDB) and destroyed (DB) buildings, both cumulated up to four different days during the considered time period

	Day 1	Day 4	Day 7	Day 10
N. ev. with $3 < M < 4$	4	9	16	25
N. ev. with $4 < M < 5$	1	2	3	7
N. ev. with $5 < M < 6$	0	0	0	0
%SDB	3.07	5.21	6.96	17.69 (8.67 masonry 9.02 reinforced concrete)
%HDB	0.2	0.58	0.91	9.09 (5.41 masonry 3.68 reinforced concrete)
%DB	0	0.28	0.51	4.49 (2.88 masonry 1.61 reinforced concrete)

related to the considered time intervals are also reported. The effects of this low intensity seismic sequence are that the majority of the buildings turn out to be undamaged at the end of the 10 days, about 17% of them results to be slightly damaged and about more than 13% are heavily damaged and destroyed. The greatest damage increment in this scenario can be observed at day 10, when the overall number of slightly, heavily damaged and destroyed buildings goes from less than 9% to more than 30% after a single earthquake of magnitude M 4.78.

It is also interesting to observe the different percentages of slightly, heavily damaged and destroyed buildings distinguished, at the end of the 10 days, for masonry and reinforced

concrete typologies. While these percentages are similar with respect to the slightly damaged condition, the number of reinforced concrete buildings highly damaged or destroyed turns out to be smaller than the correspondent values for masonry buildings.

In Fig. 7, the color map of damages for the low intensity seismic scenario is shown. The color scale is divided in seven ranges of increasing intensity. Color darkness for each municipality of the metropolitan area is proportional to the percentage of heavily damaged and destroyed buildings registered at the end of the simulation in the corresponding territory. Before the label of each municipality, the corresponding value of this percentage is also reported.

The same study has been repeated for the medium intensity seismic scenario, (characterized by 46 earthquakes of magnitude between 3 and 4, 10 between 4 and 5, and an earthquake of magnitude greater than 5). The results are reported in Fig. 8.

The figure shows the percentage of slightly damaged buildings increases almost linearly starting from the first day, going from 5%, due to a 4.02 magnitude earthquake, to 18% on the last day in correspondence with an earthquake of magnitude 5.60. The

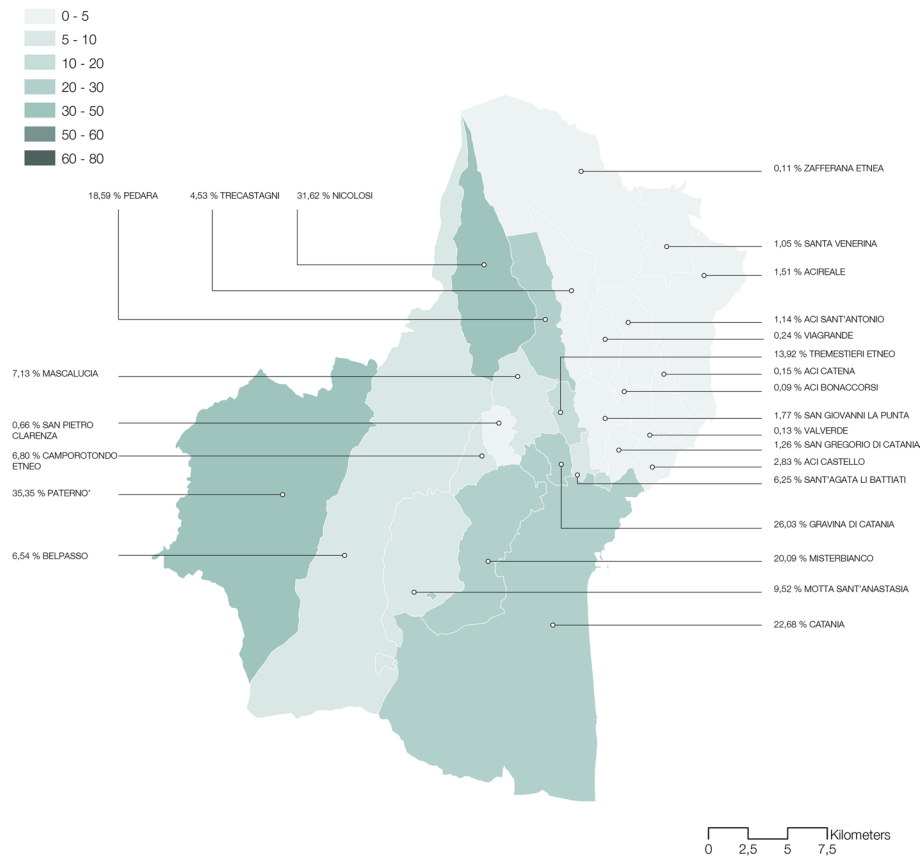


Fig. 7 Color map of damages for the low intensity scenario, with no earthquakes with $5 < M < 6$. Color intensity in the different areas of the map is proportional to the ratio between the sum of heavily damaged and destroyed buildings present in a given municipality and the corresponding total number of buildings, expressed in percentage. Values for each municipality are reported before the corresponding label

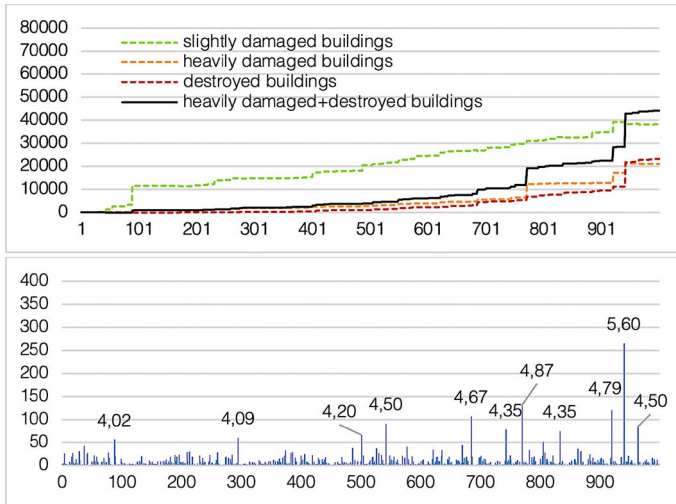


Fig. 8 Medium intensity seismic scenario: The number of damaged and destroyed buildings are reported, in the top panel, as function of 1000 seismic events, which are shown in the bottom panel

highest percentage of growth of the heavily damaged buildings and destroyed buildings occurs at day 10, where it goes from 4.50% to more than 22%, in correspondence with an earthquake of magnitude 5.60. As expected, the percentage of destroyed buildings reported in Table 7 is sensibly higher than the correspondent ones showed for the low intensity scenario. Also in this case similar percentages of slightly damaged masonry and reinforced concrete buildings can be observed at the end of the 10 days while the number of reinforced concrete buildings highly damaged or destroyed turns out to be smaller than the correspondent values for masonry buildings.

Table 7 Medium intensity seismic scenario: number of seismic events of different magnitude and percentages of slightly damaged (SDB), highly damaged (HDB) and destroyed (DB) buildings, both cumulated up to four different days during the considered time period

	Day 1	Day 4	Day 7	Day 10
N. ev. with $3 < M < 4$	8	20	35	46
N. ev. with $4 < M < 5$	1	2	5	10
N. ev. with $5 < M < 6$	0	0	0	1
%SDB	5.58	7.42	13	18.46 (9.31 masonry 9.15 reinforced concrete)
%HDB	0.44	1.00	2.68	10.15 (5.79 masonry 4.36 reinforced concrete)
%DB	0.18	0.18	2.16	11.18 (8.83 masonry 2.35 reinforced concrete)

From this scenario, it emerges that the quantity of buildings involved (SDB, HDB, DB) has increased by 20% with respect to the previous scenario. It should be noted that a moderate increase in slightly damaged corresponds to a tripled increase in the percentage of heavily damaged buildings and destroyed buildings. As for the previous scenario, in Fig. 9 the color map of damages for the medium intensity seismic scenario is also shown. Again, the color scale is divided in seven ranges of increasing intensity and color darkness is proportional to the percentage of heavily damaged and destroyed buildings registered at the end of the simulation in each territory.

Finally, a high intensity seismic scenario, with several events between M 4 and M 5, one event of M 5.24 at day 7, a second intense earthquake of M 5.88 at day 8 and one event of M 5.71 at day 10. The sequence is the same used for the calibration in Sect. 5 (applied here to the whole metropolitan area) and is reported in the bottom panel of Fig. 10, while the upper panel of the same figure shows the evolution of damages in terms of slightly damaged, heavily damaged and destroyed buildings (expressed in percentage, as usual).

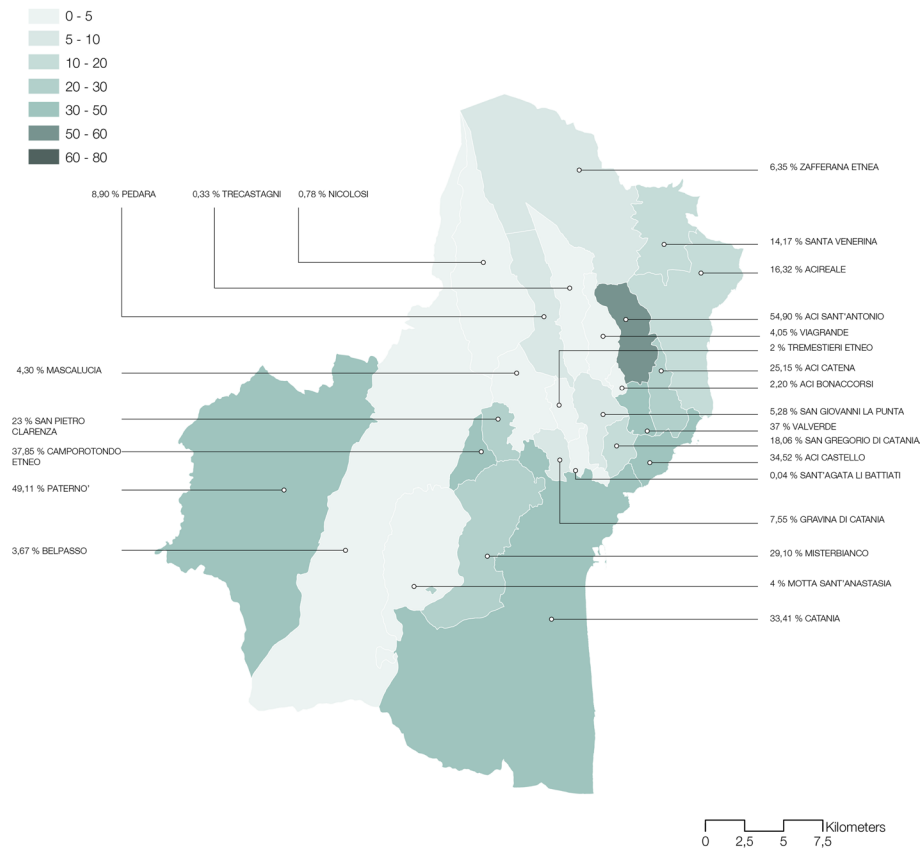


Fig. 9 Color map of damages for the medium intensity scenario, with only one earthquake with $5 < M < 6$. Color intensity in the different areas of the map is proportional to the ratio between the sum of heavily damaged and destroyed buildings present in a given municipality and the corresponding total number of buildings, expressed in percentage. Values for each municipality are reported before the corresponding label

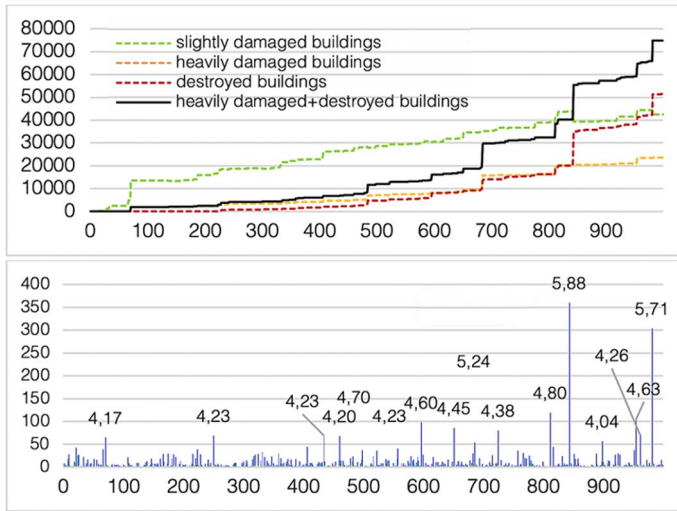


Fig. 10 High intensity seismic scenario: The numbers of damaged and destroyed buildings are reported, in the top panel, as function of 1000 seismic events, which are shown in the bottom panel

For this high intensity seismic scenario the total number of events cumulated up to days 1, 4, 7 and 10 together with the corresponding percentages of slightly damaged, highly damaged and destroyed buildings related to the considered time intervals are reported in Table 8. In this case, the percentage of slightly damaged masonry buildings at the end of the 10 days turns out to be smaller than the correspondent value for reinforced concrete ones. For higher levels of damage, similarly to what already described for the previous seismic sequences, masonry buildings are the ones more affected.

At variance of what observed for the previous seismic sequences, in this case the numbers of highly damaged and destroyed buildings are significant. The observation of Fig. 10

Table 8 High intensity seismic scenario: number of seismic events of different magnitude and percentages of slightly damaged (SDB), highly damaged (HDB) and destroyed (DEB) buildings, both cumulated up to four different days during the considered time period

	Day 1	Day 4	Day 7	Day 10
N. ev. with $3 < M < 4$	9	26	39	54
N. ev. with $4 < M < 5$	1	2	8	13
N. ev. with $5 < M < 6$	0	0	1	3
%SDB	6.52	11.03	17.07	20.51 (9.14 masonry 11.37 reinforced concrete)
%HDB	0.92	2.04	7.64	11.37 (5.82 masonry 5.55 reinforced concrete)
%DB	0	0.87	6.76	24.86 (17.391 masonry 7.47 reinforced concrete)

clearly shows that, after the end of the time interval considered, about 37% of buildings are either highly damaged or destroyed. The first main increase in the percentage of heavily damaged buildings is observed in correspondence of the shock of M 5.24, between day 6 and day 7, in which the percentage triples. Instead, the main increase in the percentage of destroyed buildings is observed in correspondence of the main shock of M 5.88, between day 8 and day 9, where the percentage increases by 4 times. The percentage of destroyed buildings reported in Table 8 confirms what one could expect, showing a further increment with respect to the medium intensity scenario. Furthermore, the map of the metropolitan area, reported in Fig. 11, shows darker colors with respect to the analogous one of the previous scenario.

The comparison of the results obtained for the three seismic sequences shows that, as expected, for all the considered ranges of parameters, the increase in the intensity of the seismic scenario produces an increase in the number of destroyed buildings. Notice that sometimes the number of slightly damaged buildings as function of time seems to decrease (for example in scenarios 2 and 3) typically in correspondence of some important seismic

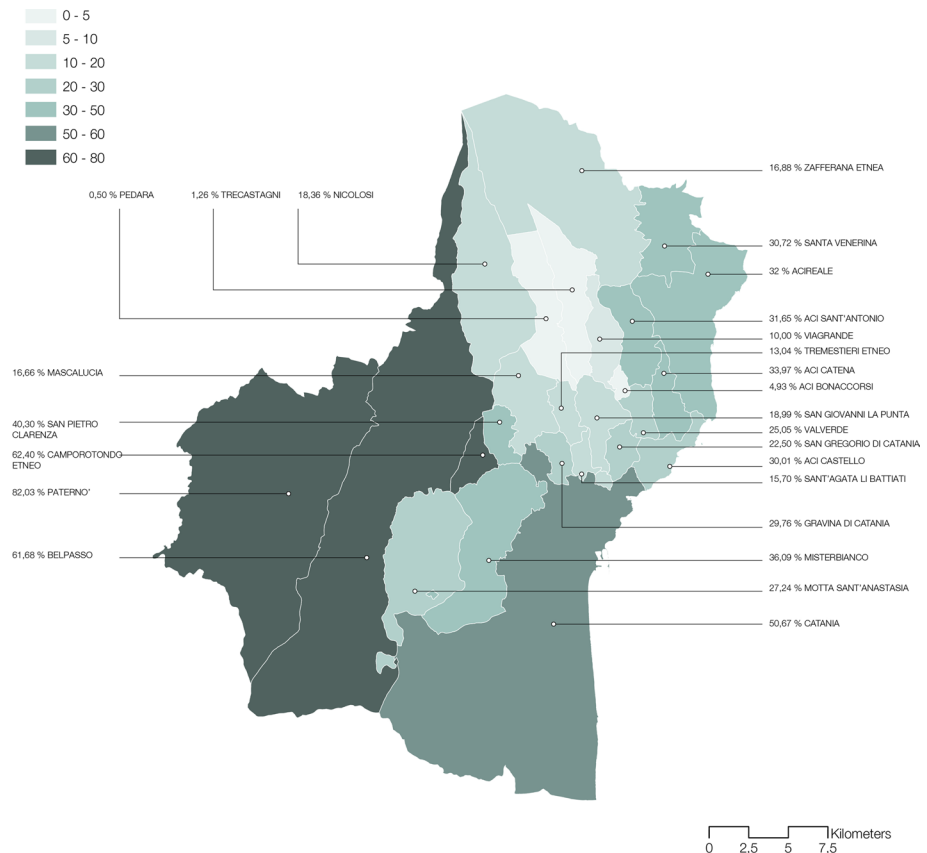


Fig. 11 Color map of damages for the high intensity scenario, with two earthquakes with $5 < M < 6$. Color intensity in the different areas of the map is proportional to the ratio between the sum of heavily damaged and destroyed buildings present in a given municipality and the corresponding total number of buildings, expressed in percentage. Values for each municipality are reported before the corresponding label

event: This is not strange and simply means that those buildings have changed status, from slightly damaged to heavily damaged or destroyed.

It also important to highlight that the system is very sensitive to its past seismic history; this means that similar seismic events may produce different damage effects because they occur at different time.

Besides the evaluation of the percentage of heavily damaged and destroyed buildings of each municipality, previously reported, the performed simulations also allow to identify in detail the location of the mostly damaged areas inside each city. Figure 12 shows for example the effects of the three considered seismic sequences on the buildings of the city of Catania. The observation of the figure clearly shows the spread of heavily damaged and destroyed buildings (marked respectively in yellow and red) when the intensity of the seismic sequence increases. The highest concentration of red points is located as expected in the oldest part of the city around the harbor. The availability of this kind of maps could represent a powerful tool in the design of appropriate emergency or risk reduction municipality plans with economic and decision-making advantages.

6.2 Single earthquakes scenarios

Let us now address a new set of three scenarios, where we consider only single major seismic events with increasing magnitude, producing damages on buildings comparable with those of the three seismic sequences previously discussed. In order to obtain statistically significant results, for each selected magnitude we repeated 100 runs starting from different initial conditions of stress over the nodes and averaged the observed damages.

Among all the simulation results, we selected three increasing values of single event magnitude each able to produce an average level of damage comparable with the one produced by each one of the three already proposed earthquake sequences. As can be seen in Table 9, the average percentage of damage, expressed as the sum of the heavily damaged and destroyed buildings, is equal to 13.45% for a single 5.63 magnitude earthquake, which is comparable to that obtained at the end of the low intensity seismic sequence (13.58%). On the other hand, a single earthquake of magnitude 6.00 produces an average damage of 21.04%, comparable with the 21.33% registered for the medium intensity scenario. Finally, the 34.80% of average damage produced by a single earthquake of magnitude 6.50 is comparable with the 36.23% of the high intensity scenario.

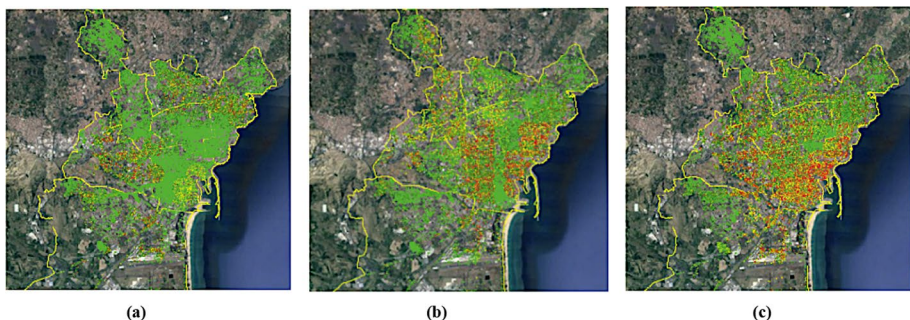


Fig. 12 Location of slightly damaged (in green), heavily damaged (in yellow) and destroyed buildings (in red) in the city of Catania. **a** low intensity scenario, **b** medium intensity scenario, **c** high intensity scenario

Table 9 Comparison between the percentages of heavily damaged buildings and destroyed buildings, averaged over three sets of 100 single earthquakes of increasing magnitude, and for the three, multiple earthquakes seismic scenarios

Single earthquake scenarios (averages over 100 runs)	%HDB	%DB	%HDB + DB
M 5.63	9.20	7.05	16.25
M 6.00	10.10	12.12	22.22
M 6.50	10.30	25.29	35.60
Multiple earthquakes scenarios	%HDB	%DB	%HDB + DB
Low intensity sequence	9.09	4.49	13.58
Medium intensity sequence	10.15	11.18	21.33
High intensity sequence	11.37	24.86	36.23

These matches confirm that the accumulation of damage on buildings deriving by repeated seismic events with moderate intensity can be considered as equivalent to a single stronger earthquake. This evidence could be of great interest for seismic prevention measures.

In Figs. 13, 14 and 15, the color maps of the metropolitan area are shown for the three single events of increasing magnitude. As usual, the various municipalities are characterized by colors organized in seven ranges of increasing intensity and assigned proportionally to the percentage of heavily damaged and destroyed buildings registered at the end of the simulation in each territory. Details of these maps can be better appreciated if discussed in comparison with the analogous ones reported in the color maps of the three multiple earthquakes scenarios. Such a comparison has been performed in Table 10, while in Fig. 16 further details concerning damages observed in each municipality for all the six considered scenarios are reported.

The low intensity multiple earthquakes scenario (with seven events with magnitude included between M 4 and M 5, and none exceeding M 5) shows, as expected, a very high percentage of municipalities, equal to 13 (52% of the 25 considered), in the first intensity range, with a percentage of heavily damaged buildings and destroyed buildings per each municipality lower than 5%. On the other hand, the single earthquake of $M=5.63$ has the largest number of municipalities equal to 14 (56%) in the third intensity range, between 10 and 20%.

The medium intensity multiple earthquakes scenario (where a few events between M 4 and M 5 and only one event above M 5) shows the largest number of municipalities in the first and in the fifth intensity ranges. Single event scenario of magnitude 6.00, similar to the medium intensity scenario for the overall percentage of heavily damaged and destroyed buildings, is characterized by a higher number of municipalities in the third and fourth interval.

Finally, the high intensity multiple earthquakes scenario is characterized by a higher number of municipalities in the third and fifth interval. This is the only scenario among those analyzed that reaches the seventh interval, consisting of 60–80% of buildings heavily damaged and destroyed for 3 (12%) of the CMA municipalities; the single event scenario of magnitude 6.50 shows the largest percentage of municipalities in the fifth interval, not reaching the last two intervals of the scale.

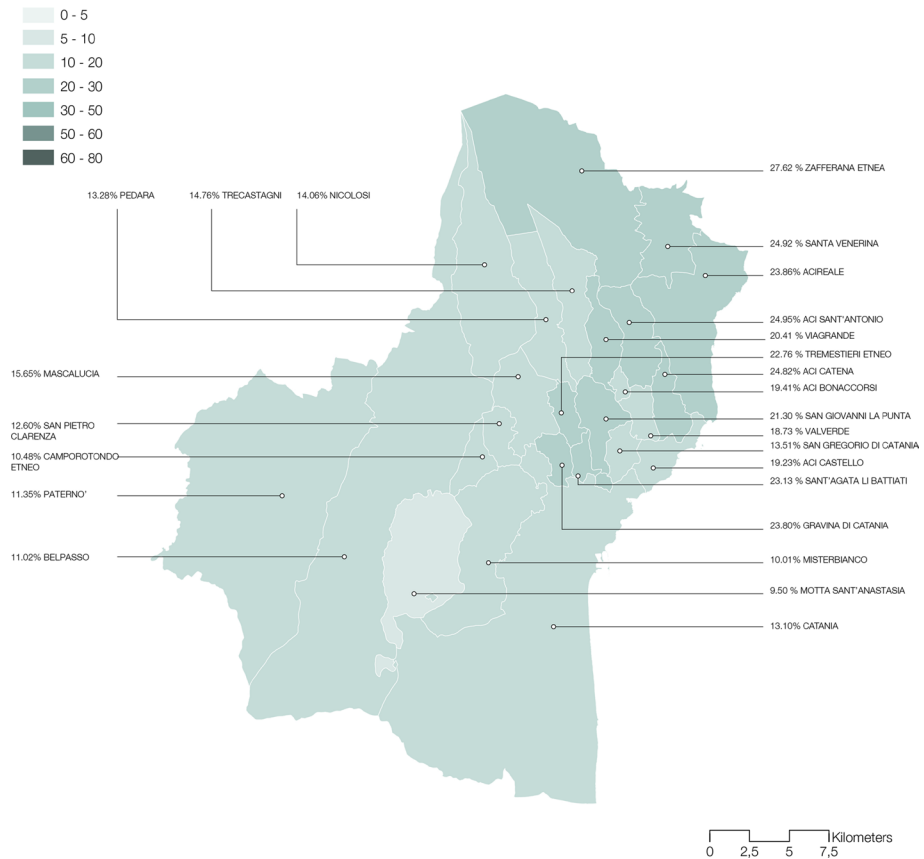


Fig. 13 Color map of damages for the single earthquake of magnitude 5.63. Color intensity in the different areas of the map is proportional to the ratio between the sum of heavily damaged and destroyed buildings present in a given municipality and the corresponding total number of buildings, expressed in percentage. Values for each municipality are reported before the corresponding label

These results allow us to conclude that the three multiple earthquakes scenarios, analyzed with the methodology adopted, cover a wider spectrum in the percentage ratio of heavily damaged and destroyed buildings if compared to what was highlighted in scenarios with single events.

Furthermore, three municipalities of the south-eastern side (Zafferana Etnea, Santa Venerina, Acireale) show the highest damage percentages (above 25% on average) in all the three single earthquake scenarios. In the innermost part, the municipalities that are most affected by the earthquake are those of the “first tier” (Gravina di Catania, Sant’Agata Li Battiati, San Giovanni La Punta, Tremestieri Etneo) with percentages between 21 and 23%. Higher percentages but similar damage behaviors are found in the case of a 6.00 magnitude earthquake and a 6.50 magnitude earthquake. Even in these cases the municipalities that are most affected by the earthquakes are those of the southeastern side of the Etna Volcano (Zafferana Etnea, Santa Venerina, Acireale, Aci Sant’Antonio, Aci Catena) with average percentages ranging between 26 and 32%, and 38% and 46% in the case of 6.00 and 6.50 magnitude earthquake, respectively. The percentages of “first tier” municipalities range

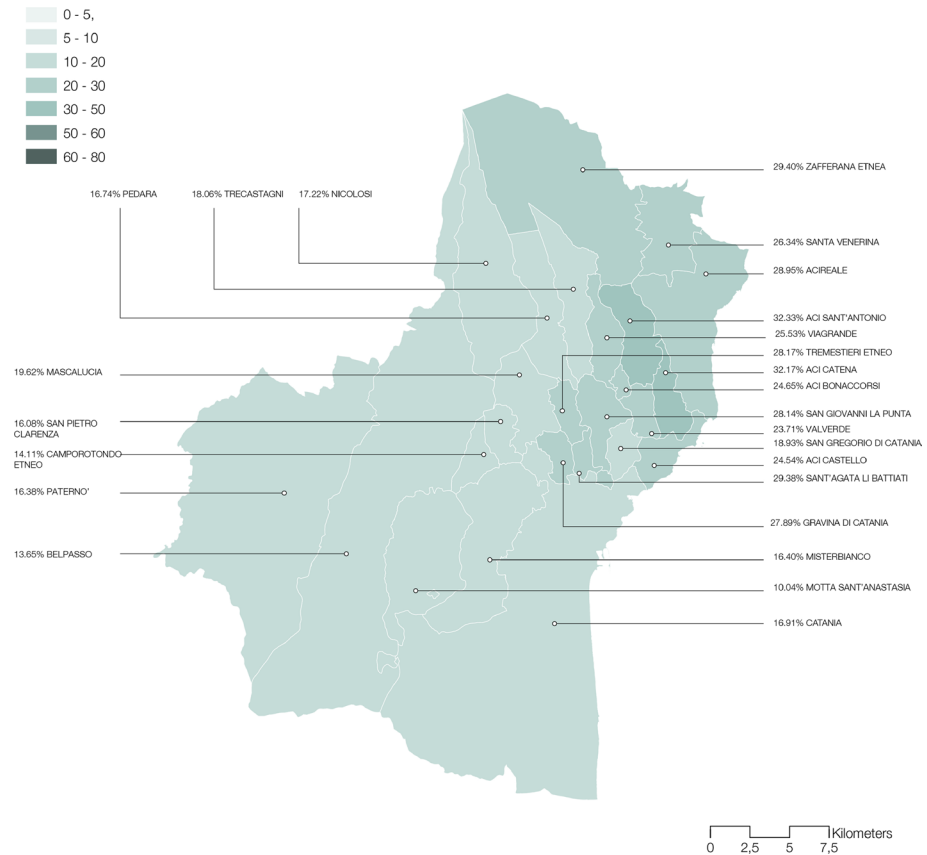


Fig. 14 Color map of damages for the single earthquake of magnitude 6.00. Color intensity in the different areas of the map is proportional to the ratio between the sum of heavily damaged and destroyed buildings present in a given municipality and the corresponding total number of buildings, expressed in percentage. Values for each municipality are reported before the corresponding label

between 25 and 30% and between 43 and 46% in the case of the 6.00 and 6.50 magnitude earthquake, respectively.

7 A-priori risk index

In the previous chapters we considered the impact of seismic events (sequences or single) in terms of the percentages of damaged buildings in the various municipalities. However, being the number of buildings in each municipality very different, in order to quantify the real impact and the total damage due to seismic events, one should consider the number of damaged/destroyed buildings. In this section, we present this new analysis introducing an a-priori risk index. General risk assessment theory relies on “Crichton’s Risk Triangle” (CRT) (Crichton 1999; Kron and Wu 2002). This approach has been initially adopted in the insurance industry (Crichton 1999) and then applied to spatially distributed risk assessment in fields related to disaster management, such

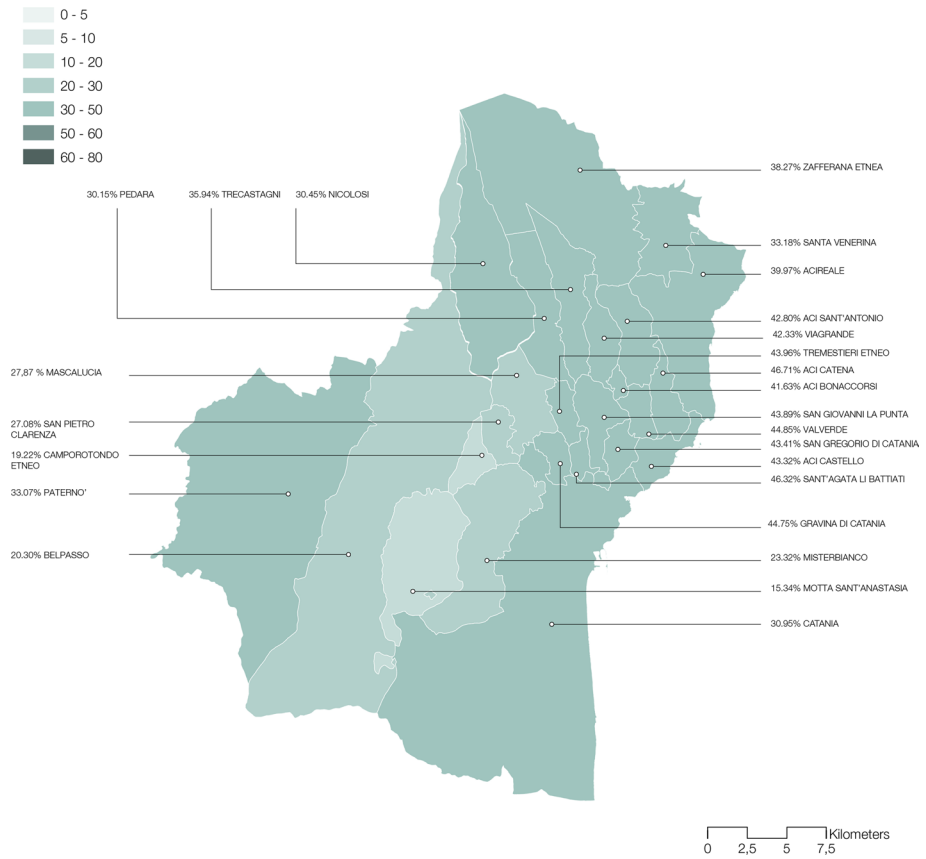


Fig. 15 Color map of damages for the single earthquake of magnitude 6.50. Color intensity in the different areas of the map is proportional to the ratio between the sum of heavily damaged and destroyed buildings present in a given municipality and the corresponding total number of buildings, expressed in percentage. Values for each municipality are reported before the corresponding label

Table 10 Number of CMA municipalities (out of the 25 considered) which present a percentage of heavily damaged and destroyed buildings included in the various ranges of damage intensity

Intensity ranges	1°	2°	3°	4°	5°	6°	7°
%HDB + DB	0–5%	5–10%	10–20%	20–30%	30–50%	50–60%	60–80%
Low intensity sequence	13	5	2	3	2	–	–
Single event M 5.63	–	1	14	1	–	–	–
Medium intensity sequence	9	4	3	3	5	1	–
Single event M 6.00	–	–	12	11	2	–	–
High intensity sequence	3	–	7	4	7	1	3
Single event M 6.50	–	–	2	3	20	–	–

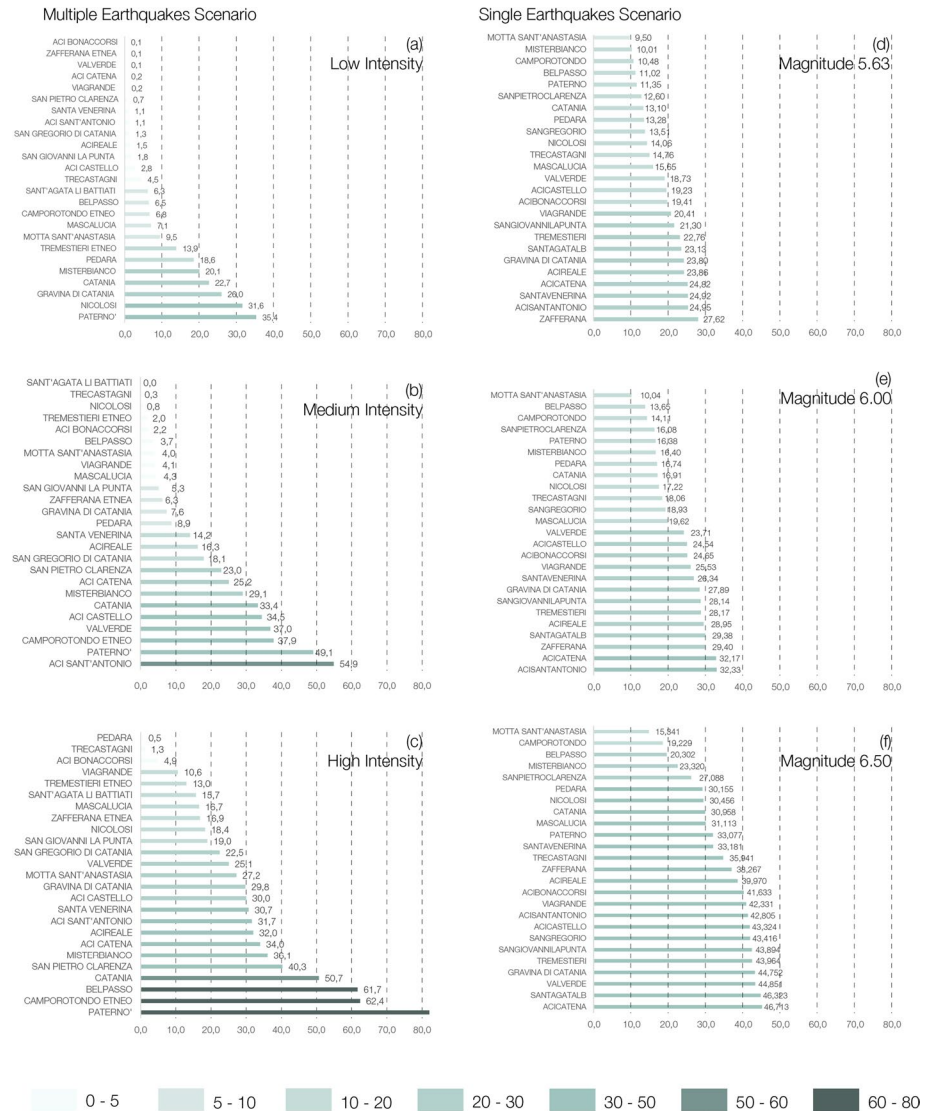


Fig. 16 Multiple Earthquakes Scenarios: **a** low intensity; **b** medium intensity; **c** high intensity. Single earthquakes scenarios: **d** magnitude 5.63; **e** magnitude 6.00; **f** magnitude 6.50. For each of the six scenarios, details of the percentage of highly damaged and destroyed buildings for all the municipalities in the Catania metropolitan area are reported

as climate change impact (Tomlinson et al. 2011; IPCC 2014; Thomalla et al. 2006; Kim et al. 2015; Collins et al. 2009; Estoque et al. 2020) or earthquakes (Babayev et al. 2010). In the CRT framework, risk is calculated as a function of 3 main components: Hazard, Exposure and Vulnerability. Hazard expresses the potential for an event to produce harm (e.g., earthquake, epidemics, flooding); Exposure evaluates the amount of assets exposed to harm (e.g., buildings, population, infrastructures); Vulnerability

represents the attitude of those assets to be damaged when exposed to hazard events (e.g., building characteristics, age of population, drainage systems).

For the aim of this paper, we will consider Hazard (H) as proportional to the impact of a generic strong earthquake on buildings and affected by factors related to geological characteristics of the municipality area, in particular the average ground acceleration, the average slope and the presence of faults. Exposure (E) will be proportional to the number of resources who might potentially be damaged or destroyed by the earthquake, i.e., the number of buildings present in that municipality. Finally, Vulnerability (V) will be proportional to the most expressed initial vulnerability (mode) of buildings present in the municipality.

More in detail, we define, for the k -th municipality ($k = 1, \dots, 25$):

$$H_k = \frac{1}{3} \frac{\langle a_g \rangle_k}{\max[\langle a_g \rangle_k]} + \frac{1}{3} \frac{\langle a_s \rangle_k}{\max[\langle a_s \rangle_k]} + \frac{1}{3} \frac{(N_f)_k}{\max[(N_f)_k]} \tag{4}$$

$$E_k = \frac{(N_b)_k}{\max[(N_b)_k]} \tag{5}$$

$$V_k = \frac{\text{Mode}(V_0)_k}{\max[\text{Mode}(V_0)_k]} \tag{6}$$

where: $\langle a_g \rangle_k$ is the ground acceleration a_g averaged over the sites of the k -th municipality; $\langle a_s \rangle_k$ is the slope a_s averaged over the sites of the k -th municipality; $(N_f)_k$ is the number of “fault nodes” of the OFC network included in the k -th municipality; $(N_b)_k$ is the number of buildings present in the k -th municipality; $\text{Mode}(V_0)_k$ is the mode of the initial vulnerability of the buildings present in the k -th municipality.

All the considered quantities in Eqs. (4), (5) and (6) have been normalized to their maximum values over the 25 municipalities.

Finally, the risk index R_k which characterizes the k -th municipality is easily obtained as the product of the three components of the risk triangle (multiplicative model):

$$R_k = H_k \cdot E_k \cdot V_k \tag{7}$$

and will be normalized to its maximum value over all the municipality in order to have values included in the interval $[0, 1]$. Since this index has been built on the basis of geological and building stock data not related with a specific earthquake, we can also call it “a-priori” risk index, since it can be considered as a sort of prediction of the a-priori risk level of a certain geographical area.

In Table 11, the ranking of the 25 municipalities present in the CMA (left column) is reported according to decreasing values of the a-priori normalized risk index R_k (central column). Looking at the ranking, we can easily identify four classes of municipalities characterized by a different aggregated level of risk: Catania and Acireale are in the first class, with a “very high” a-priori risk level, $R_k > 0.5$; immediately below, four municipalities, namely Misterbianco, Paternò, Belpasso and Mascalucia, are labeled with an “high” level of risk, $0.2 < R_k < 0.5$; then, a group of 10 municipalities with $0.1 < R_k < 0.2$ are classified with a “medium” risk level; finally, a group of the last 9 municipalities are labeled with a “low” risk level, for $R_k < 0.1$.

Of course, these predictions about the aggregated a-priori risk level of the considered municipalities need to be compared with the “a-posteriori” damages observed in the same

Table 11 Risk ranking of the 25 municipalities of the Catania metropolitan area compared with the corresponding average damage resulting from our numerical simulations as effect of the three major single seismic events of magnitude M 5.63, M 6.00 and M 6.50 (each one repeated 100 times to obtain a statistical relevance)

	Municipality	Risk index	Av. damage over 3 seismic events	
Very high risk	Catania	1.00	10401	
	Acireale	0.74	5870	
High risk	Misterbianco	0.30	2291	
	Paterno'	0.28	2736	
	Belpasso	0.25	1801	
	Mascalucia	0.23	2728	
Medium risk	Pedera	0.17	1588	
	Trecastagni	0.16	1309	
	Nicolosi	0.15	1130	
	Sangiovanilapunta	0.15	2705	
	Acicatena	0.15	1814	
	Motta Sant'anastasia	0.14	695	
	Zafferana	0.14	1377	
	Acisantantonio	0.14	2328	
	Acicastello	0.13	1495	
	Gravina Di Catania	0.12	1630	
	Low risk	Tremestieri	0.09	1611
		Santavenerina	0.08	937
Viagrande		0.07	966	
Valverde		0.05	856	
Santagatalb		0.04	811	
Acibonaccorsi		0.04	614	
Sanpietroclarenza		0.03	393	
Camporotondo		0.02	170	
Sangregorio	0.01	501		

The four risk groups identified by the risk index values are in very good agreement with the observed damages (only three municipalities have been underestimated, since have been classified in the risk group immediately below the right one)

municipalities, as they result from our numerical simulations. In this regard, we decided to take into account the results coming from the single earthquakes scenarios, which—thank to the average over 100 repetitions—have a greater statistical significance.

In the last column of Table 11 we report, for each municipality, the number of buildings heavily damaged or destroyed, averaged over the three single earthquakes scenarios with, respectively, magnitude M 5.63, M 6.00 and M 6.50. These values represent the average response of a given number of buildings, present on a given territory and exposed to a seismic hazard, toward the occurrence of a strong earthquake. As one can see, the four a-priori risk groups are able to account for the a-posteriori average damage quite well: actually, only three municipalities, San Giovanni La Punta, Aci Sant'Antonio and Tremestieri (text in red), result to have been underestimated (of one class only) by the prediction of our risk index. This risk ranking analysis reveals the municipalities at higher risk toward major seismic events in terms of the average number of buildings heavily damaged or destroyed, at variance with what discussed in the previous chapter, where only the percentage of the damaged buildings inside the municipalities was considered. Obviously, municipalities

with a higher number of buildings have in general a higher propensity toward the possibility to have a more severe impact and so a higher risk.

8 Conclusions

In the present paper, we investigated the seismic risk of metropolitan areas simulating earthquakes by means of a modified Olami–Feder–Christensen (OFC) model, in the context of self-organized criticality (Olami et al. 1992; Jensen 1998). We took into account also some geological features in the evaluation of the seismic intensities perceived by each single building. A large territory in the Sicilian oriental coast, the Catania metropolitan area, which includes several urbanized zones with different features, was considered as case study. First, we presented applications of the procedure with reference to seismic sequences of variable intensity, which are rather frequent in seismic territories. We showed that the damage can be progressively accumulated in the buildings and may lead to their collapse even when the intensities of each single event are moderate. As a second step, we studied statistically significant simulations of single major seismic events, equivalent to a given sequence in terms of produced damages on buildings. Finally, we introduced a novel a-priori index able to characterize the seismic risk of each single municipality in the considered metropolitan area. The predictions based on this index results to be in a very good agreement with the results of numerical simulations. In particular, the evaluation of the damage produced by the simulated ground motions on the buildings of the considered territory and the new risk index we introduced, allow to characterize in a quantitative way the most vulnerable areas and therefore to plan appropriate measures for risk management.

The simulations here presented show that the examined area is characterized by high seismic risk. This condition has been aggravated by the lack of proper consideration of seismic hazard in land use planning and the consequent release of building consents. This happened especially during the long season of tumultuous development that took place between 1960s and late 1980s. In this period, decision makers purposely underestimated the relevance of this risk, giving priority to the development of the construction industry. Today, the awareness of the relevance of this issue is by all means higher than in the past, but effective actions are urgently needed in order to implement sound policies aimed at reducing seismic risk. The study here presented gives some hints for setting up these policies, i.e., for guiding the definition of priorities in the allocation of funds for upgrading the most vulnerable buildings. In particular, it is evident that municipalities lying in higher positions in the proposed a-priori risk index ranking should be prioritized in the allocation of funds. The adoption of such a decision tool would represent a novelty for risk policies in Italy, since public subsidies are currently assigned taking into account only hazard and vulnerability, without explicit reference to exposure.

Author contributions AG, AP contributed to conceptualization; AG, EF and AP contributed to methodology; AP and EF contributed to software; AG and AP contributed to validation; EF, AG and AP contributed to investigation; EF, GB, FM contributed to resources; EF, GB, FM contributed to data curation; EF, AG and AP contributed to writing—original draft preparation; EF, AG, AP and AR contributed to writing—review and editing; AG and AP contributed to visualization; AG, AP, AR contributed to supervision; AG, AP and AR contributed to funding acquisition.

Funding Open access funding provided by Università degli Studi di Catania within the CRUI-CARE Agreement. This research was partially funded by the University of Catania, with the projects “Linea di intervento 2 Piano PIA.CE.RI 2020/2022 ” of the Departments of Civil Engineering and Architecture and Physics

and Astronomy “Ettore Majorana” and by the Italian Ministry of University and Research (MUR) with the projects “PRIN2017 linea Sud: Stochastic forecasting in complex systems” and PRIN2020 #20209F3A37.

Declarations

Conflict of interest The authors declare no conflict of interest. The funders had no role in the design of the study; in the collection, analyses, or interpretation of data; in the writing of the manuscript, or in the decision to publish the results.

Open Access This article is licensed under a Creative Commons Attribution 4.0 International License, which permits use, sharing, adaptation, distribution and reproduction in any medium or format, as long as you give appropriate credit to the original author(s) and the source, provide a link to the Creative Commons licence, and indicate if changes were made. The images or other third party material in this article are included in the article’s Creative Commons licence, unless indicated otherwise in a credit line to the material. If material is not included in the article’s Creative Commons licence and your intended use is not permitted by statutory regulation or exceeds the permitted use, you will need to obtain permission directly from the copyright holder. To view a copy of this licence, visit <http://creativecommons.org/licenses/by/4.0/>.

References


- Allen J, Balrlow J, Leal J, Maloutas T, Padovani L (2004) Housing and welfare in southern Europe. Blackwell Publishing, Oxford
- Ambraseys NN, Simpson KA, Bommer JJ (1996) Prediction of horizontal response spectra in Europe. *Earth Eng Struct Dyn* 25:371–400
- Azzaro R, Lo Giudice E, Rasa R (1989) Catalogo degli eventi macrosismici e delle Catalogo degli eventi macrosismici e delle fenomenologie da creep nell’area etnea dall’agosto 1980 al dicembre 1989. *Boll Gruppo Nazionale Vulcanol* 1:13–46
- Azzaro R, D’Amico S, Tuvè T (2011) Estimating the magnitude of historical earthquakes from macroseismic intensity data: new relationships for the volcanic region of Mount Etna (Italy). *Seismol Res Lett* 82(4):520–531
- Azzaro R, Bonforte A, Branca S, Guglielmino F (2013) Geometry and kinematics of the fault systems controlling the unstable flank of Etna volcano (Sicily). *J Volcanol Geotherm Res* 251:5–15
- Babayev G, Ismail-Zadeh A, Le Mouél JL, Contadakis ME (2010) Scenario-based earthquake hazard and risk assessment for Baku (Azerbaijan). *Nat Hazards Earth Syst Sci* 10(12):2697–2712
- Baiesi M, Paczuski M (2004) Scale-free networks of earthquakes and aftershocks. *Phys Rev E* 69:066106. <https://doi.org/10.1103/PhysRevE.69.066106>
- Bard P-Y, Bouchon M (1985) The two-dimensional resonance of sediment-filled valleys. *Bull Seismol Soc Am* 75:519–541
- Bard P-Y, Campillo M, Chavez-Garcia FJ, Sanchez-Sesma FJ (1988) A theoretical investigation of large- and small-scale amplification effect in the Mexico City valley. *Earthq Spectra* 4–3:609–633
- Barreca G, Bonforte A, Neri M (2013) A pilot GIS database of active faults of Mt. Etna (Sicily): a tool for integrated hazard evaluation. *J Volcanol Geotherm Res* 251:170–186. <https://doi.org/10.1016/j.jvolgcores.2012.08.013>
- Bonforte A, Puglisi G (2006) Dynamics of the eastern flank of Mount Etna volcano (Italy) investigated by a dense GPS network. *J Volcanol Geotherm Res* 153:357–369
- Bonforte A, Guglielmino F, Coltelli M, Ferretti A, Puglisi G (2011) Structural assessment of Mount Etna volcano from permanent scatterers analysis. *Geochem Geophys Geosyst* 12:Q02002. <https://doi.org/10.1029/2010GC003213>
- Bosi A, Marazzi F, Pinto A, Tsionis G (2011) The L’Aquila (Italy) earthquake of 6 April 2009: report and analysis from a field mission. Scientific and Technical Research Reports, Publications Office of the European Union 978-92-79-18990-6
- Boukri M et al (2018) Seismic vulnerability assessment at urban scale: case of Algerian buildings. *Int J Disaster Risk Reduct* 31:555–557
- Branca S, Ferrara V (2013) The morphostructural setting of Mount Etna sedimentary basement (Italy): implications for the geometry and volume of the volcano and its flank instability. *Tectonophysics* 586:46–64. <https://doi.org/10.1016/j.tecto.2012.11.011>
- Branca S, Coltelli M, De Beni E, Wijbrans J (2008) Geological evolution of Mount Etna volcano (Italy) from earliest products until the first central volcanism (between 500 and 100 ka ago) inferred from

- geochronological and stratigraphic data. *Int J Earth Sci* 97(1):135–152. <https://doi.org/10.1007/s00531-006-0152-0>
- Carocci CF (2012) Small centres damaged by 2009 L'Aquila earthquake: on site analyses of historical masonry aggregates. *Bull Earthq Eng* 10:45–71
- Caruso F, Pluchino A, Latora V, Vincipiguerra S, Rapisarda A (2007) A new analysis of self-organized criticality in the OFC model and in real earthquakes. *Phys Rev E* 75:055101(R)
- Chiodelli F, Coppola A, Belotti E, Berruti G, Clough Marinaro I, Curci F, Zanfi F (2020) The production of informal space: a critical atlas of housing informalities in Italy between public institutions and political strategies. *Prog Plan* 100495:1–40
- Collins TW, Grineski SE, Aguilar MDLR (2009) Vulnerability to environmental hazards in the Ciudad Juárez (Mexico)–El Paso (USA) metropolis: a model for spatial risk assessment in transnational context. *Appl Geogr* 29(3):448–461
- Crichton D (1999) The risk triangle. Natural disaster management: a presentation to commemorate the International Decade for Natural Disaster Reduction (IDNDR) 1990–2000. *Ingleton J: Tudor Rose*
- Decanini LD, Liberatore L, Mollaioli F (2012) Damage potential of the 2009 L'Aquila, Italy, earthquake. *J Earthq Tsunami* 6(3):1250032
- Del Gaudio C, Ricci P, Verderame GM (2015) Development and urban-scale application of a simplified method for seismic fragility assessment of RC buildings. *Eng Struct* 91:40–57
- Del Gaudio C, Di Ludovico M, Polese M et al (2020) Seismic fragility for Italian RC buildings based on damage data of the last 50 years. *Bull Earthq Eng* 18:2023–2059. <https://doi.org/10.1007/s10518-019-00762-6>
- Dibben CJL (2008) Leaving the city for the suburbs—the dominance of 'ordinary' decision making over volcanic risk perception in the production of volcanic risk on Mt Etna, Sicily. *J Volcanol Geotherm Res* 172:288–299
- Dogliani C, Innocenti F, Mariotti S (2001) Why Mt. Etna. *Terra Nova* 13(1):25–31. <https://doi.org/10.1046/j.1365-3121.2001.00301.x>
- EMS. European Macroseismic Scale (1998) Conseil de l'Europe. European Seism. Commission. 8 LUX-EMBOURG 1998
- Estoque RC, Ooba M, Seposo XT, Togawa T, Hijioka Y, Takahashi K, Nakamura S (2020) Heat health risk assessment in Philippine cities using remotely sensed data and social-ecological indicators. *Nat Commun* 11(1):1–12
- Ferreira TM, Rodrigues H, Vicente R (1996) Seismic vulnerability assessment of existing reinforced concrete buildings in urban centers. *Sustainability* 2020:12. <https://doi.org/10.3390/su12051996>
- Fischer E, Biondo AE, Greco A, Martinico F, Pluchino A, Rapisarda A (2022) Objective and perceived risk in seismic vulnerability assessment at an urban scale. *Sustainability* 14:9380. <https://doi.org/10.3390/su14159380>
- Froger JL, Merle O, Briole P (2001) Active spreading and regional extension at Mount Etna imaged by SAR interferometry. *Earth Planet Sci Lett* 148:245–258
- Gambino S, Barreca G, Gross F, Monaco C, Ktastel S, Gutscher MA (2021) Deformation pattern of the northern sector of the Malta escarpment (Offshore SE Sicily, Italy): fault dimension, slip prediction, and seismotectonic implications. *Front Earth Sci* 8:594176. <https://doi.org/10.3389/feart.2020.594176>
- Gómez-Bernal A, Peña AR, Gil JA (2023) Probabilistic seismic vulnerability and loss assessment of the buildings in Mexico City. *IntechOpen*
- Greco A, Pluchino A, Cannizzaro F (2020a) A novel procedure for the assessment of the seismic performance of frame structures by means of limit analysis. *Bull Earthq Eng* 18(9):4363–4386
- Greco A, Lombardo G, Pantò B, Famà A (2018) Seismic vulnerability of historical masonry aggregate buildings in oriental Sicily. *Int J Arch Herit*. <https://doi.org/10.1080/15583058.2018.1553075>
- Greco A, Pluchino A, Barbarossa L, Barreca G, Calìo I, Martinico F, Rapisarda A (2019) A new agent-based methodology for the seismic vulnerability assessment of urban areas. *ISPRS Int J Geo-Inf* 8(6):274
- Greco A, Fiore I, Occhipinti G, Caddemi S, Spina D, Calìo I (2020b) An equivalent non-uniform beam-like model for dynamic analysis of multi-storey irregular buildings. *Appl Sci (Switzerland)* 10(9):3212
- Gutscher M, Dominguez S, Mercier de Lepinay B, Pinheiro L, Gallais F, Babonneau N, Cattaneo A, Le Faou Y, Barreca G, Micallef A, Rovere M (2016) Tectonic expression of an active slab tear from high-resolution seismic and bathymetric data offshore Sicily (Ionian Sea). *Tectonics* 35:39–54. <https://doi.org/10.1002/2015TC003898>
- Gvirtzman Z, Nur A (1999) Formation of Mount Etna as a consequence of slab rollback. *Nature* 401(6755):782–785
- Hancilar U, Tuzun C, Yenidogan C, Erdik M (2010) ELER software—a new tool for urban earthquake loss assessment. *Nat Hazard*. <https://doi.org/10.5194/nhess-10-2677-2010>
- Hoyos MC, Hernandez AF (2022) Seismic risk assessment of multiple cities: biases in the vulnerability derivation methods for urban areas with different hazard levels. *Front Earth*. <https://doi.org/10.3389/feart.2022.910118>

- IPCC (2014) Synthesis report, contribution of working groups I, II and III to the fifth assessment report of the intergovernmental panel on climate change, 2014, IPCC, Geneva, Switzerland
- Jaimes DL, Escudero CR, Flores KL et al (2022) Multicriteria seismic hazard and social vulnerability assessment in the Puerto Vallarta metropolitan area, Mexico: toward a comprehensive seismic risk analysis. *Nat Hazards*. <https://doi.org/10.1007/s11069-022-05783-0>
- Jensen HJ (1998) Self-organized criticality: emergent complex behavior in physical and biological systems. Cambridge University Press
- Kawashima K, Aydan O, Aoki T, Kisimoto I, Konagai K, Matsui T, Sakuta J, Takahashi N, Teodori S, Yashima A (2010) Reconnaissance investigation on the damage of the 2009 L'Aquila, central Italy earthquake. *J Earthq Eng* 14:816–841
- Kim H, Park J, Yoo J, Kim TW (2015) Assessment of drought hazard, vulnerability, and risk: A case study for administrative districts in South Korea. *J Hydro-Environ Res* 9(1):28–35
- Kossobokov VG, Nekrasova A (2017) Characterizing aftershock sequences of the recent strong earthquakes in central Italy. *Pure Appl Geophys* 174:3713–3723. <https://doi.org/10.1007/s00024-017-1624-9>
- Kron W (2002) Flood risk = hazard x exposure x vulnerability. In: Wu M et al (eds) Flood defence. Science Press, New York, pp 82–97
- Lagomarsino S, Giovinazzi S (2006) Macroseismic and mechanical models for the vulnerability and damage assessment of current buildings. *Bull Earthq Eng* 4:415–443
- La Greca P, Martinico F (2017) Città metropolitana di Catania. In: De Luca G, e Moccia FD (a cura di), Pianificare le città metropolitane in Italia. Interpretazioni, approcci, prospettive, pp 421–452, INU Edizioni
- La Greca P, Barbarossa L, Ignaccolo M, Inturri G, Martinico F (2011) The density dilemma. A proposal for introducing smart growth principles in a sprawling settlement within catania metropolitan area. *Cities* 28(6):527–535. <https://doi.org/10.1016/j.cities.2011.06.009>
- La Rosa SD, Privitera R (2013) Characterization of non-urbanized areas for land-use planning of agricultural and green infrastructure in urban contexts. *Landscape and Urban Planning* 109:94–106
- Lin J, Smerzini C (2022) Variability of physics-based simulated ground motions in Thessaloniki urban area and its implications for seismic risk assessment. *Front Earth Sci*. <https://doi.org/10.3389/feart.2022.951781>
- Lundgren P, Casu F, Manzo M, Pepe A, Berardino P, Sansosti E, Lanari R (2004) Gravity and magma induced spreading of Mount Etna volcano revealed by satellite radar interferometry. *Geophys Res Lett*. <https://doi.org/10.1029/2003GL018736>
- Lu XZ, Han B, Hori M, Xiong C, Xu Z (2014) A coarse-grained parallel approach for seismic damage simulations of urban areas based on refined models and GPU/CPU cooperative computing. *Adv Eng Softw* 70:90–103
- Maio R, Vicente R, Formisano A, Varum H (2015) Seismic vulnerability of building aggregates through hybrid and indirect assessment techniques. *Bull Earthq Eng* 13(10):2995–3014
- Maio R, Ferreira TM, Vicente R (2016) A critical discussion on the earthquake risk mitigation of urban cultural heritage assets. *Int J Disaster Risk Reduct* 27:239–247
- Malagnini L, Akinci A, Herrmann RB, Pino NA, Scognamiglio L (2002) Characteristics of the ground motion in northeastern Italy. *Bull Seismol Soc Am* 92(6):2186–2204
- Malagnini L, Herrmann RB, Di Bona M, M. (2000) Ground motion scaling in the Apennines (Italy). *Bull Seismol Soc Am* 90(4):1062–1081
- Matassoni L, Giovinazzi S, Pollino M, Fiaschi A, La Porta L, Rosato VA (2017) Geospatial decision support tool for seismic risk management: Florence (Italy) case study. In: Gervasi O, et al. (ed) Computational science and its applications—ICCSA 2017. ICCSA 2017. Lecture Notes in Computer Science, vol 10405. Springer, Cham
- Meletti C, Montaldo V, Stucchi M, Martinelli F (2006) Database della pericolosità sismica MPS04. Istituto Nazionale di Geofisica e Vulcanologia (INGV)
- Musson RMW, Grunthal G, Stucchi M (2010) The comparison of macroseismic intensity scales. *J Seimol* 14:413–428
- NTC (2008) Nuove Norme Tecniche per le Costruzioni. D.M. 14/01/2008. G.U. n.29 del 04/02/2008 (Suppl. Ordinario n. 30)
- Olami Z, Feder HJS, Christensen K (1992) Self-organized criticality in a continuous, nonconservative cellular automaton modeling earthquakes. *Phys Rev E* 68(8):1244–1247
- Omori F (1894) On the aftershocks of earthquakes. *J Coll Sci Imp Univ Tokyo* 7:111–200
- Polese M, Di Ludovico M, Prota A, Manfredi G (2013) Damage-dependent vulnerability curves for existing buildings. *Earthq Eng Struct Dyn* 42:853–870

- Puglisi G, Bonforte A (2004) Dynamics of Mount Etna volcano inferred from static and kinematic GPS measurements. *J Geophys Res* 109:B11404
- Ramos LF, Lourenço PB (2004) Modelling and vulnerability of historical city centres in seismic areas: a case study in Lisbon. *Eng Struct* 26(9):1295–1310
- Rasà R, Azzaro R, Leonardi O (1996) Aseismic creep on faults and flank instability at Mt. Etna Volcano, Sicily. *Geol Soc Lond Spec Publ* 110:179–192
- Riedel I, Guéguen P, Dalla Mura M et al (2015) Seismic vulnerability assessment of urban environments in moderate-to-low seismic hazard regions using association rule learning and support vector machine methods. *Nat Hazards* 76:1111. <https://doi.org/10.1007/s11069-014-1538-0>
- Rovida A, Locati M, Camassi R, Lolli B, Gasperini P (2016) CPTI15, the 2015 version of the parametric catalogue of Italian earthquakes Rome, Italy: Istituto Nazionale di Geofisica e Vulcanologia
- Rust D, Neri M (1996) The boundaries of large-scale collapse on the flanks of Mount Etna, Sicily. *Geol Soc Lond Spec Publ* 110:193–208
- Sabetta F, Pugliese A (1996) Estimation of response spectra and simulation of nonstationarity earthquake ground motion. *Bull Seismol Soc Am* 86:337–352
- Saunders W, Kivilgton M (2016) Innovative land use planning for natural hazard risk reduction: a consequence-driven approach from New Zealand. *Int J Disaster Risk Reduct* 18:244–255
- Senaldi I, Magenes G, Penna A (2010) Numerical investigations on the seismic response of masonry building aggregates. *Adv Mater Res* 133:715–720
- Silva V, Horspool N (2019) Combining USGS shakemaps and the openquake-engine for damage and loss assessment. *Earthq Eng Struct Dyn* 48:1–19. <https://doi.org/10.1002/eqe.3154>
- Stefanov D, Solakov D, Milkov J (2023) Assessment of the effects of strong earthquakes on the city of Plovdiv. In: IOP Conference Series: Materials Science and Engineering, Vol 1276. IOP Publishing, p 012008
- Stucchi M, Meletti C, Montaldo V, Akinci A, Faccioli E, Gasperini P, Malagnini L, Valensise G (2004). Pericolosità sismica di riferimento per il territorio nazionale MPS04. Istituto Nazionale di Geofisica e Vulcanologia (INGV). <https://doi.org/10.13127/sh/mps04/ag>
- Thomalla F, Downing T, Spanger Siegfried E, Han G, Rockström J (2006) Reducing hazard vulnerability: towards a common approach between disaster risk reduction and climate adaptation. *Disasters* 30(1):39–48
- Tomlinson CJ, Chapman L, Thornes JE, Baker CJ (2011) Including the urban heat island in spatial heat health risk assessment strategies: a case study for Birmingham, UK. *Int J Health Geogr* 10(1):42
- Utsu T, Ogata Y, Matsu'ura RS (1995) The centenary of the Omori formula for a decay law of aftershock activity. *J Phys Earth* 43:1–33
- Vargas-Alzate YF, Lantada N, González-Drigo R, Pujades LG (2020) Seismic risk assessment using stochastic nonlinear models. *Sustainability* 12:1308. <https://doi.org/10.3390/su12041308>
- Vicente R, Ferreira T, Maio R (2014) Seismic risk at the urban scale: assessment. *Mapp Plan Procedia Econ Financ* 18:71–80
- Watts DJ, Strogatz SH (1998) Collective dynamics of 'small world' networks. *Nature* 393:440
- Zhai Y, Chen S, Ouyang Q (2019) GIS-based seismic hazard prediction system for urban earthquake disaster prevention planning. *Sustainability* 11:2620. <https://doi.org/10.3390/su11092620>
- Zhao Z, Zhao Z, Jiren Xu, Kubota R, Liu L (2007) Strong ground motion simulation for seismic hazard assessment in an urban area. *J Geophys Eng* 4(3):308–316. <https://doi.org/10.1088/1742-2132/4/3/S10>
- Zuccaro G, Cacace F (2015) Seismic vulnerability assessment based on typological characteristics. The first level procedure "SAVE." *Soil Dyn Earthq Eng* 69:262–269

Authors and Affiliations

Eliana Fischer¹  · **Giovanni Barreca**² · **Annalisa Greco**³ · **Francesco Martinico**⁴ · **Alessandro Pluchino**^{1,5} · **Andrea Rapisarda**^{1,5,6}

✉ Eliana Fischer
eliana.fischer@phd.unict.it

Giovanni Barreca
giovanni.barreca@unict.it

Annalisa Greco
annalisa.greco@unict.it

Francesco Martinico
francesco.martinico@unict.it

Alessandro Pluchino
alessandro.pluchino@ct.infn.it

Andrea Rapisarda
andrea.rapisarda@ct.infn.it

¹ Department of Physics and Astronomy “Ettore Majorana”, University of Catania, Via Santa Sofia, 64, 95123 Catania, Italy

² Department of Biological, Geological and Environmental Science, University of Catania, Corso Italia, 57, 95129 Catania, Italy

³ Department of Civil Engineering and Architecture, University of Catania, Via Santa Sofia, 64, 95123 Catania, Italy

⁴ Dipartimento di Agricoltura, Alimentazione, Ambiente, University of Catania, Via Santa Sofia, 100, 95123 Catania, Italy

⁵ INFN sezione di Catania, via Santa Sofia 64, 95123 Catania, Italy

⁶ Complexity Science Hub, Vienna, Austria